UNIVERSITÄT LEIPZIG

Fakultät für Physik und Geowissenschaften der Universität Leipzig

Knotty or Nice? Identification and Characterization of Protostellar Outflows in *Spitzer* c2d Images

Katherine Guenthner

Master's Thesis

submitted January 2009

Erstgutachter: Prof. Dr. rer. nat. Tilman Butz
Zweitgutachter: Dr. Jens Kauffmann

Hiermit erkläre ich, dass ich die Masterarbeit selbständig verfasst habe und keine anderen als die angegebenen Quellen und Hilfsmittel benutzt habe. Alle Stellen der Arbeit, die wrtlich oder sinngem aus Veröffentlichungen oder aus anderweitigen fremden Äußerungen entnommen wurden, sind als solche kenntlich gemacht. Ferner erkläre ich, dass die Arbeit noch nicht in einem anderen Studiengang als Prüfungsleistung verwendet wurde.

_____

Ich bin einverstanden, dass die Arbeit nach positiver Begutachtung in der Universitätsbibliothek zur Verfügung steht.

_____

I hereby certify that this master's thesis has been composed by myself, and describes my own work, unless otherwise acknowledged in the text. All references and verbatim extracts have been quoted, and all sources of information have been specifically acknowledged. It has not been accepted in any previous application for a degree.

_____

After positive appraisal of this thesis, I agree that one copy of my presented thesis may remain at the disposal of the library of Leipzig University.

_____

ABSTRACT

We use near to mid-infrared data from the *Spitzer Space Telescope* to study outflows from young stellar objects in five known star formation regions in our galaxy. The simultaneous collection of data by instruments aboard Spitzer is used to characterize both the outflow and its driving source. I present an extensive and unbiased statistical study of these outflows and their sources found in so-called giant molecular cloud complexes.

As a star forms, it ejects mass in an energetic outburst known as an outflow. Our understanding of these outflows is based on a rather large and varied number of studies, many of which from the last decade. Protostellar outflows appear as knot-like extended structures in near-infrared (3.6–8.0μm) images from the *Spitzer Space Telescope*, that emanate from embedded young stellar objects (YSO), which are also well-characterized in mid-infrared bands. Using the extensive survey by the group "From Molecular Cores to Planet Forming Disks" of the five molecular clouds, we are able to closely examine outflows and their suspected drivers in a homogeneous and ultimately unprecedented way, since observations of these objects are traditionally in optical or radio wavelengths and of a mixed nature. Our strategy is to manually inspect the images of the clouds, searching for and marking typical features of outflow nebulosity, using this mark-up as a guide for tracing the extent of the outflows to the suspected outflow source.

From our method of careful inspection, we identify and characterize 86 outflow lobes extending from their sources. Of these we consider 42% to have the highest confidence rating. We can organize the total number of outflows into 45 different outflow systems consisting of at least one lobe. From this, we find 58% of these are considered as bipolar, or have at least one lobe on each side of the generating star. We also find relationships between protostellar and outflow properties. For example, from analysis of the spectral energy distributions of the central sources, we can determine the protostellar bolometric temperature, which is a measure of circumstellar obscuration, and luminosity and associate them to properties of outflows. We find that outflow sources are more likely to have a bolometric temperature of $T_{\rm bol} < 10^2$ K, and spectral slopes of $\alpha \geq 1$. This tells us that outflow driving YSOs are more reddened and cooler than the full YSO sample in these clouds. From this analysis, we also confirm that outflow sizes are characteristic of a particular phase of young star formation and that analyzing their sizes provides robust age information about their source.

Contents

1. Introduction to Star Formation

People have always wondered about the nature of stars, and more recently how they form. But for many years the study of their formation was only a theoretical one. With the advent of infrared and radio astronomy, due mainly to advances in instrumentation, an empirical description of star formation could begin to take shape. Astronomers could now peer through the obscuring dust and observe the inner depths of molecular clouds, places where stars were believed to be born. Infrared observations of IRAS (Infrared Astronomical Satellite) revealed that many of the dense cores identified by radio observations had point-like IR sources within them. The presence of these suspected young stars was direct evidence that it was in these cold gaseous cores that stars did indeed form. Detailed maps in radio wavelengths also showed the existence of bipolar lobes of gas emanating from these central sources, and it is now believed that this outflow phase is a fundamental aspect of star formation.

The basic approach then to studying the formation and development of stars has been to gather and classify various physical properties of young stellar objects (YSO) to understand how they change from one set of properties to another. From this we can see the four basic evolutionary steps (Shu, Adams, & Lizano 1987) in the production of low-mass stars like our Sun are:

1. A slowly rotating dense cloud core forms.

2. The core collapses into a protostar and disk, and is surrounded by an infalling envelope of material.

3. A strong stellar wind produces collimated jets and a bipolar outflow.

4. The wind sweeps away the circumstellar material, revealing the YSO, and the disk condenses into a planetary system.

In the following, I describe early observations of molecular clouds and their fragmentation which generates dense cores in Sect. 1.1 (step 1 from above), in Sect. 1.2 we discuss the different phases of young stellar objects (2), and Sect. 1.3 reviews the outflow phase, which is the primary focus of the work presented here (3).

1.1. Molecular Clouds

The vast space between stars in our galaxy is not entirely empty, but contains material known as the interstellar medium (ISM). Gas and dust are the two largest components of the ISM, and ultimately form the environment from which stars are born. The dust makes up about 1% of the total mass of the ISM, but is much more opaque than the gas. Dust particles absorb light with wavelengths smaller than their diameters ($\sim$0.1 μm), and reradiate this energy in the infrared. This means that dusty regions will effectively block out the blue part of the spectrum of the light

that passes through them, making them appear redder (Zeilik & Gregory 1998). This is known as interstellar reddening, or extinction A, and is measured in magnitudes at the observed wavelength. The rest of the mass of the ISM is composed of various species of interstellar gas, cold and dilute, which also absorb and emit at characteristic wavelengths. That is, the dust and gas prevent us from directly observing objects that are embedded in the densest regions of the ISM, in our case the inner regions of dense clouds where stars form. Though very thin, interstellar gas can accumulate under its own gravitation and form a dense region. These regions are commonly referred to as molecular clouds, and are mostly seen in the spiral arms of our galaxy. Figure 1 shows well-known clouds in our galaxy.

Molecular clouds were first seen as dark patches in the sky that seemed to have no stars. In the early twentieth century, observations suggested that instead of being starless, these regions were "dark nebulae" that obscured starlight, and carefully constructed photographic catalogs were made of all these objects (Barnard 1919). We now know that these nebulae are composed primarily of molecular hydrogen H_2, but the name "molecular clouds" did not appear till radio observations identified CO molecules within these objects (Wilson et al. 1970). Carbon monoxide, the second most abundant molecule, acts as a tracer, since less energy is required to collisionally excite the rotational transition of CO. Thus, most maps of molecular clouds are made with the J$= 1 - 0$ rotational transition line of the CO molecule, at $\lambda = 2.6$ mm. Indeed, large-scale surveys in CO of the Galactic plane discovered that there were many molecular clouds in our galaxy, and advances in detectors showed that they had a varied substructure (Dame et al. 1987). It is important to note that the clouds also contain a small amount of dust. Dust grains, responsible for the darkness of molecular clouds (the extinction of starlight) emit thermal radiation in the infrared and microwave regimes ($\lambda \approx 100$ to 1000 μm), which provides another method to examine the molecular cloud structure.

As with many things in nature, molecular clouds come in many different shapes and sizes. Larger clouds are called giant molecular clouds (GMC), whereas smaller clouds (sometimes called dark clouds) are grouped together into molecular clouds complexes. GMCs have average temperatures of around 15 K, densities up to 100 cm^{-2}, and can be upwards of 50 pc in size.[a] These giant clouds have masses of 10^4–10^6 solar masses[b] ($M_\odot$), but the distribution of mass is extremely non-uniform, and matter again congregates into clumps (Shu et al. 1987). The densest part of these clumps are called dense cores (or Bok globules). Cores have temperatures of about 10 K, densities of $n \geq 10^4$ cm^{-2}, and are only fractions of a parsec in length. Figure 2 shows the hierarchical structure within a larger molecular cloud. The dense cores of molecular clouds is where the exciting story of star formation begins.

---

[a] 1 pc $= 3.09 \times 10^{13}$ km.

[b] 1 $M_\odot = 1.988 \times 10^{30}$ kg

Fig. 1.— Simplified view of some molecular clouds in the Northern sky. The extent of the clouds is indicated by *dark gray*, with the backdrop of the Milky Way in *light gray*. Several constellations and bright stars are also marked. The upper darkened region is the Taurus-Auriga Cloud Complex. The Orion Molecular Cloud (the lower dark gray region) has an angular size of 15° on its longest axis, which is around 120 pc at a distance of 450 pc. From Stahler & Palla (2005)

1.2. Dense Cores and Protostars

Stars are known to be born from the gravitational contraction of interstellar molecular clouds of gas and dust, but we do not as of yet clearly understand this process. We can however say that the general picture of the star formation process begins with the collapse of the dense cloud core. Accordingly, we limit the discussion to describing an ideal case, spherically symmetric collapsing core, omitting magnetic effects, which should not change even after more details become available. The initial conditions for collapse are these (from Shu, Adams, & Lizano 1987): consider a cloud of gas that is nearly isothermal and rotating slowly. The growing concentration of material at the center of the cloud will almost always cause a spontaneous collapse to occur from the inside-out. That is, the central regions collapse more rapidly than outer parts and a condensation quickly forms at the center (see middle column in Fig. 3). Further compression of this central lump will then cause the internal temperature to rise steadily, and by the ideal gas law $PV = nkT$, the pressure must therefore rise as well. The central condensed material is referred to as a protostar or young stellar object (YSO), where the dense material just outside the protostar is known as the circumstellar envelope. Material continues to fall inward toward the protostar, but due to

conservation of angular momentum, a disk forms around the nascent star (Terebey et al. 1984). This is generally referred to as the circumstellar disk. In this work we will refer to the protostellar system as including the envelope, disk and protostar. Matter now in the disk will continue to move inward and eventually accrete onto the protostar. Figure 2 shows a schematic picture of a collapsing dense core with a YSO, girded by a circumstellar disk, sitting at the center of a star forming region. One problem with this simplified view of the Shu model of collapse, in that it assumes that only the center contracts and ultimately causes the *inside-out* collapse of the dense core. However, the infall motion of starless cores in molecular clouds in surveys conducted by Lee et al. (1999, 2001, 2004) show global contraction motions, that is, the inward motions of the gas do not necessarily occur just at the center. Thus, the initial conditions for the formation of stars in these cores require more study.

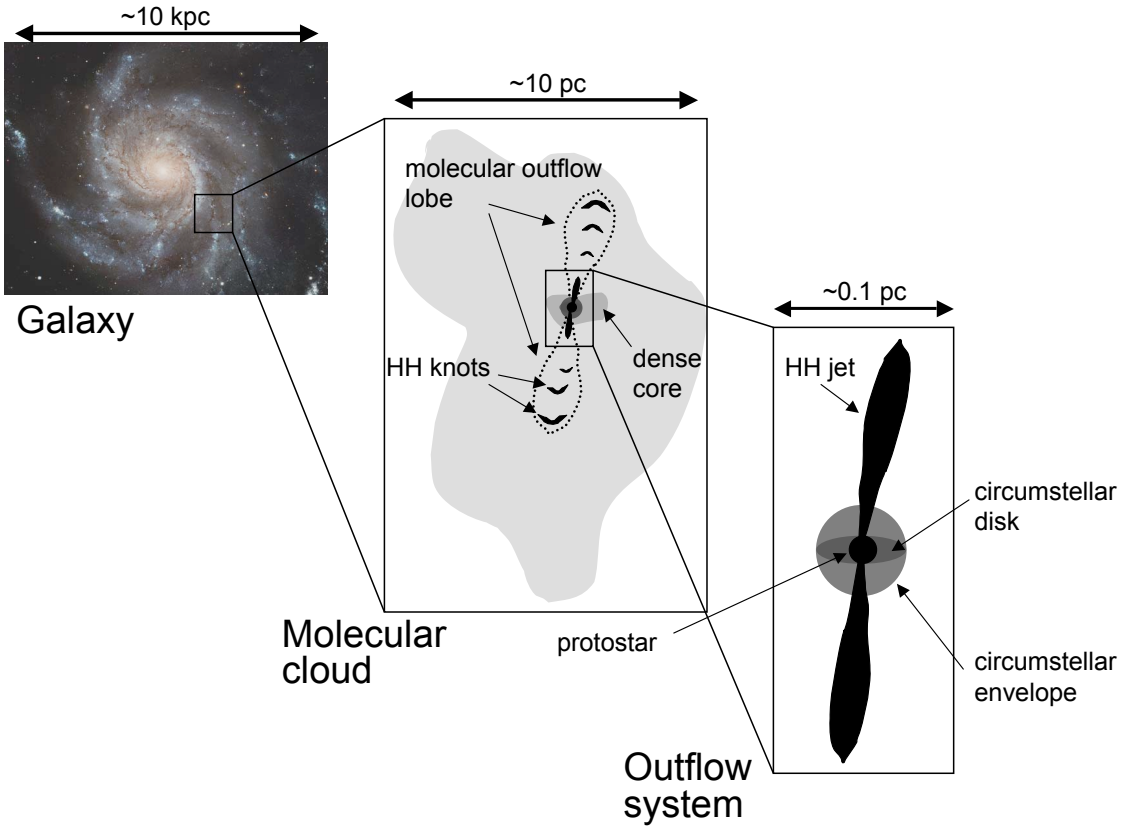

Fig. 2.— Hierarchical structure of molecular cloud (not to scale). The star forming dense core within the cloud is shown in the center figure, with the various components

It is apparent that molecular clouds and cores have some inherent rotation, and therefore must conserve angular momentum (Caselli et al. 2002). We can show this in a simple example, by looking at the conservation of angular momentum for a core, $m_{\rm i} v_{\rm i} r_{\rm i} = m_{\rm f} v_{\rm f} r_{\rm f}$. Here we assume a radius $r_{\rm i}$ of 0.1 pc ($3\ \times 10^{15}$ m), a mass of 1 $M_{\odot}$ (using radius of the Sun; $7\ \times 10^{8}$ m) with no mass-loss, $m_{\rm i} = m_{\rm f}$, and rotational velocity of $v_{\rm i} = 1$ km s^{-1}. If we solve, we find $v_{\rm f} = v_{\rm i}(r_{\rm i}/r_{\rm f}) = 1\ {\rm km\,s^{-1}}(3 \times 10^{15}\,{\rm m}/7 \times 10^{8}\,{\rm m}) \approx 5 \times 10^{6}\ {\rm km\,s^{-1}}$, which is larger than the speed of light (!), and obviously points to a mechanism that a protostar must use in order to relieve some angular momentum before it becomes a main sequence star, i.e., before it reaches hydrostatic equilibrium and derives its energy from fusion. It is therefore assumed that as the growing star accumulates more and more mass from the circumstellar disk, the systems then expels mass in the form of a bipolar flow, seen as two streams moving in opposite directions from the source and aligned with the star's rotational axis (Bally & Lada 1983). The work by Bacciotti et al. (2002) and more recently by Chrysostomou et al. (2008), showed that jets emerging from embedded objects do indeed rotate, and more observational evidence for this shedding of mass and extra angular momentum is discussed in Sect. 1.3.

1.2.1. Energy Distribution of Protostars

We now explore the current working model of star formation and the different phases of protostars, eventually leading to the stage where they begin to expel accreted material in the form of molecular outflows. Here we also discuss the two schemes used to gauge the age of the protostar by examining their energy distribution. We discussed above that although protostars do not have the critical mass necessary to ignite their cores, the act of material accreting onto the central source from the circumstellar disk still produces a large amount of energy. We know from the virial theorem that the gravitational contraction of a mass results in half of the potential energy ($2E_{\rm thermal} = -U$) being radiated away as the star's luminosity. The energy per unit time (power) released by the infalling gas as it lands on the surface of the star is the accretion luminosity:

$$\begin{aligned} L_{\rm acc} &\equiv \frac{GM_{*}\dot{M}}{R_{*}}\ , \\ &= 61\ L_{\odot}\left(\frac{\dot{M}}{10^{-5} M_{\odot}\ {\rm yr^{-1}}}\right)\left(\frac{M_{*}}{1\ M_{\odot}}\right)\left(\frac{R_{*}}{5\ R_{\odot}}\right)^{-1}\ . \end{aligned} \tag{1}$$

We let $\dot{M} = 1 \times 10^{-5}\ M_{\odot}$ yr^{-1}, and $M_{*} = 1\ M_{\odot}$, where G, M_{*}, $\dot{M}$, and R_{*} are the gravitational constant ($= 6.67\ \times 10^{-11}$ m^{3} kg^{-1} s^{-2}), the mass of the protostar, the mass rate (M_{*}/t), and the radius of the protostar, respectively (Shu, Adams, & Lizano 1987). $M_{\odot}$, $R_{\odot}$, and $L_{\odot}$ are the solar mass, the solar radius, and the solar luminosity. Equation 1 says that $L_{\rm acc}$ is the that essentially all the kinetic energy of the infall is converted into radiation, which is valid for low-mass star formation with spherical symmetry. The surrounding halo of cold, optically thick dust will

absorb this stellar radiation, and re-emit at its own characteristic wavelengths. This results in a spectral energy distribution (SED) that is shifted to peak in the infrared (reddened), as compared to main-sequence stars that have energy profiles closer to blackbodies. SEDs, normally a plot of λF_λ, versus wavelength, λ, of light, are constructed from observations over a wide wavelength range and essentially are the combination of emission from all three components of the protostellar system (central accreting star, circumstellar disk, infalling spherical envelope).

From the work by Lada & Wilking (1984) in their broadband study from 2 to 20 μm of the embedded population of IR sources in the Ophiuchi dark cloud, the important outcome was that each stage of star formation could be divided into morphological classes based on the shape of their spectral energy distributions. Example SEDs from the work by Lada and Wilking, and a thorough explanation of the class system are found in Fig. 3. From these spectra, three distinct classes (I through III) could be identified. Note here is that we use the general terminology of "stage" to describe a physical configuration of the protostellar system, and "class" to describe the SED. Later a Class 0 was added to include deeply embedded sources that are only detected at far-infrared or millimeter wavelengths (Andre et al. 1993), as seen in the uppermost spectrum in Fig. 3. We see from Wien's displacement law that thermal radiation which peaks at 10μm has an associated temperature near 300 K, which corresponds to dust thermal emission as we would expect for a deeply embedded object. The general rule being that the more infrared radiation, the larger amount of cooler material surrounding the star, indicating that the protostar is still condensing and in an earlier stage of development (Lada & Wilking 1984; Lada 1987). It follows then that we can use the infrared excess (shift of SED into the IR) as an empirical measure of stellar youth. If one takes the slope of the SED around 10 μm, this slope is known as the spectral index, and is calculated from

$$\alpha = \frac{d\log(\lambda F_\lambda)}{d\log\lambda} \ . \tag{2}$$

Further refinement of the class system came from Greene et al. (1994) who formalized a 4-class system, and added a "flat" spectrum category to the picture. The spectral index α, which depends on the range of wavelengths used and varies in the literature, for each class α can be written as the following (from Evans et al. 2008):

I	$0.3 \leq \alpha$
Flat	$-0.3 \leq \alpha < 0.3$
II	$-1.6 \leq \alpha < -0.3$
III	$\alpha < -1.6$

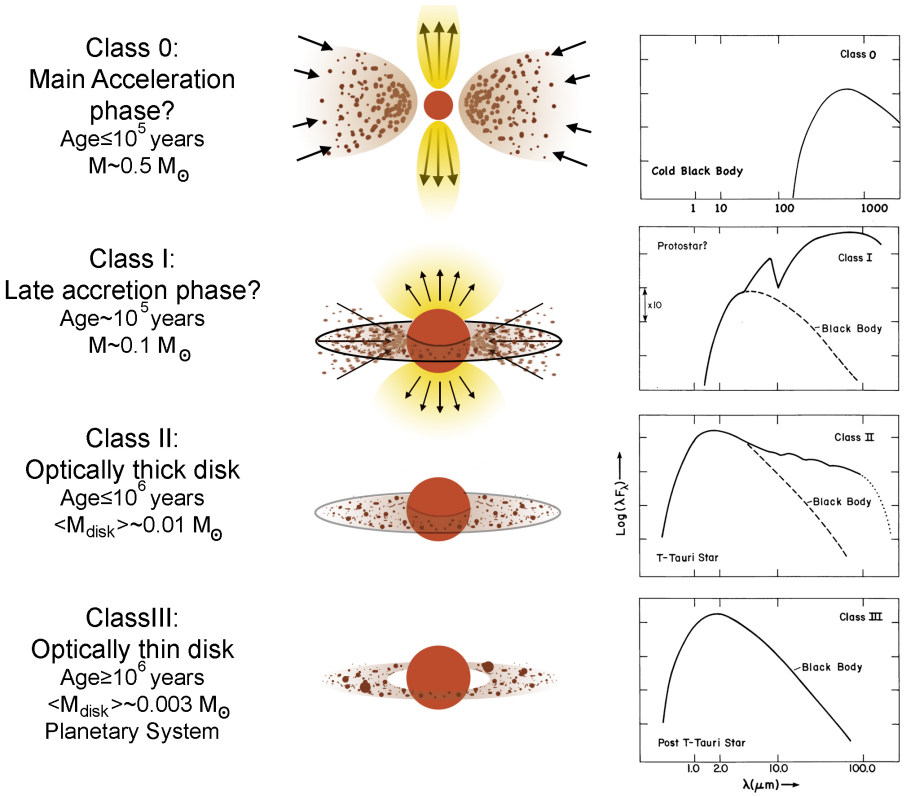

Fig. 3.— Specific phases of star formation. The spectral energy distributions on the right match up with each stage of stellar evolution in the center. The spectrum profiles for Class I to Class III seen here resemble those first observed by Lada & Wilking (1984), with Class 0 added for completeness. In star formation, a molecular cloud begins to collapse where local inhomogeneities cause matter to condense. This produces friction which produces light. Due to spherical asymmetry in condensation, the collapsing clump begins to rotate. The medium surrounding this star forming core of material filters the YSO light, producing a very low $T_{\rm bol}$, where at this protostellar stage $T_{\rm bol} < T_{\rm eff}$ (SED like the top spectrum of **Class 0**). The core continues to condense and rotation accelerates. Again from the conservation of momentum, $L = mvr$, as the mass of the YSO increases, the angular momentum must also increase. Thus the YSO emits polar jets, which dissipate this increase in the YSO's angular momentum. Material continues to accrete onto the YSO, which depletes the surrounding cloud allowing more YSO light to escape without being reddened, thus $T_{\rm bol}$ increases, coming closer to $T_{\rm eff}$ (**Class I**). As the YSO grows in size, it must also slow its speed of rotation, thus the jet loses it's collimation and disperses surrounding material reducing accretion (**Class II**). Eventually accretion onto the YSO and outflow cease, leaving a circumstellar disk of non-accreted material that will form the planetary system. Since the majority of the cloud has been accreted onto the YSO, the YSO's light becomes significantly less filtered, and $T_{\rm bol} \approx T_{\rm eff}$ and we would see a blackbody-shaped SED as for **Class III** sources.

The spectral index is not listed for Class 0 objects because they could not be observed at the wavelengths originally used for classification, thus Class 0 are included in Class I numbers. We can characterize an optically visible star by two parameters: its bolometric luminosity, $L_{\rm bol}$, and effective temperature, $T_{\rm eff}$. The bolometric luminosity measures the radiant energy flux of the star and is obtained by integrating over all observed fluxes, and is given in units of solar luminosities $L_\odot$.[c] The effective temperature is defined as the temperature of a blackbody that has the same radius and energy flux as the star. Using these two properties, one can create a version of the Hertzsprung–Russell diagram (H-R), by plotting log-log of $L_{\rm bol}$ versus $T_{\rm eff}$. The H-R diagram is of great importance to the understanding of stellar evolution, where certain locations on the plot precisely relate to stellar properties such as mass, age and composition. However, the diagram only describes "mature" stars that have reached the main sequence and is less useful for earlier stages of stellar development such as the YSO stage. This is due to the fact that many YSO are still embedded in their parent dust and gas envelopes and this obscures optical measurements of $T_{\rm eff}$ (Myers & Ladd 1993).

To remedy this, Myers & Ladd (1993) suggested the use of a bolometric temperature $T_{\rm bol}$ to characterize YSOs. Bolometric temperature is defined as the temperature of a blackbody with the same mean frequency $\bar{\nu}$ as the measured SED of the source, and is a measure of circumstellar obscuration. We also use the construct of $T_{\rm bol}$ as an indicator of the development of a YSO. $T_{\rm bol}$ and $L_{\rm bol}$ can be calculated as in Myers & Ladd (1993):

$$T_{\rm bol} \equiv \frac{\zeta(4)}{4\zeta(5)}\frac{h\bar{\nu}}{k} = 1.25 \times 10^{-11}\bar{\nu}({\rm K\ Hz^{-1}}) \tag{3}$$

where h is Planck's constant, k is Boltzmann's constant, $\zeta(n)$ is the Riemann ζ function of argument n, and the mean frequency $\bar{\nu}$ is the ratio of the first and zeroth moments of the spectrum of the source F_ν, which gives some measure of the "redness" of an observed SED (Ladd et al. 1991):

$$\bar{\nu} = \frac{\int_0^\infty \nu F_\nu\ d\nu}{\int_0^\infty F_\nu\ d\nu}\ , \tag{4}$$

The bolometric luminosity is given by:

$$L_{\rm bol} = 4\pi D^2 \int_0^\infty F_\nu d\nu\ , \tag{5}$$

where D is the distance to the source. Chen et al. (1995) then showed that the classes used to characterize YSOs had specific ranges of $T_{\rm bol}$ [K]:

0	$T_{\rm bol} < 70$
I	$70 \leq T_{\rm bol} \leq 650$
II	$650 < T_{\rm bol} \leq 2800$

[c] $1\ L_\odot = 3.846 \times 10^{26}$ W

1.3. Protostellar Outflow Phase

Outflows from young stellar systems can be seen over a wide range of wavelengths, from the UV to radio. Observations of molecules around these systems revealed high-speed flows of gas, and it is now clear that most protostars will undergo a phase of energetic mass-loss along the disk's rotational axis in the form of a bipolar outflow: two streams moving in opposite directions. Lasting only thousands of years (Eisloeffel & Mundt 1994), this display happens in a blink of an eye in stellar terms, which makes it an exciting snapshot of star formation in action. Interestingly, these striking phenomena were not predicted by star formation theorists and are still a topic astronomers struggle to understand. We can understand these objects in the following way (Bally et al. 2007): The YSO accelerates a wind, which is sometimes collimated into a jet. This primary jet and wind transfer momentum and sweep up some ambient material by means of shock waves propagating into the medium. The secondary shocks have lower velocities than the jets and can be seen in H_2 emission (near-IR) when the shock front interacts with the surrounding molecular cloud. This interaction can also be detected in Hα or forbidden line emission (optical) when the medium is atomic or ionized. Molecular line emission observed at submillimeter to centimeter wavelengths (radio) is mostly produced by gas entrained by the secondary shock waves. Therefore, there is not a single tracer that reveals the entire outflow story, i.e., each tracer provides information concerning only a limited set of physical conditions. In the following I discuss how we are approaching a more complete view of outflow phenomena by studying various manifestations of protostellar outflows across many portions of the electromagnetic spectrum.

1.3.1. HH Objects and Shocks

The mass-loss process manifests itself in various forms. One type is the phenomena known as Herbig–Haro (HH) objects. Herbig and Haro independently were the first to observe these objects more than half a century ago, when they noticed that two nebulous objects located in nearby dark clouds also had unusual spectra (Herbig 1951; Haro 1952). In addition to Hα, these strange objects emitted a broad continuum and a number of forbidden optical transitions such as [S II], [N II], and [O III]. Later, in the 1970s, their spectra were interpreted as signposts of shock waves, which occur when fast, ejected gas in the form of a stellar wind collides with the surrounding medium causing it to glow (Schwartz 1975). A chain of HH objects is generally referred to as an HH flow, or if more compact and closer to the protostar, known as an HH jet (see Fig. 4). Speeds of up to 300 km s^{-1} were found for HH flows, with HH jet velocities reaching up to around 500 km s^{-1}. Most HH objects lie within 0.5 pc of their parent star (jets are closer yet), with very few found more than 1 pc away. However, some HH objects have been observed to lie several parsecs away from their source, which may imply that the interstellar medium is not very dense in their vicinity, allowing them to travel further from their source before dispersing (Bally 2007). As of now, over 400 individual HH objects or groups are known, most associated with star forming regions (Reipurth 2000).

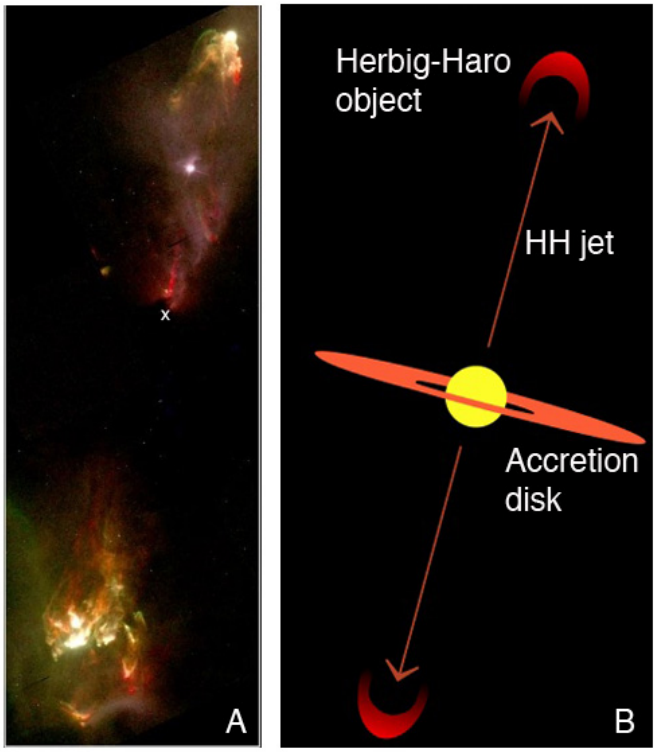

Fig. 4.— **A** Optical image of HH 1 and HH 2, which lie in the Orion Molecular Cloud. A composite made from Hubble Space Telescope data: Hα line at 6563 Å(green), [S II] (red) and a broadband continuum filter (blue). The source VLA1 is marked by an cross. If we look back to Fig. 1, we see that the Orion Molecular Cloud is about 15° along its longest dimension, or 120 pc in length. The outflow formed by HH 1 and HH 2 is only a few tenths of a parsec. **B** Simplified view of HH objects. From J. Hester (Arizona State University), NASA

As an example we look to the first two HH objects discovered, HH 1 and HH 2 (Fig. 4). We see there that the objects sit on opposite sides of their driving source, known as VLA 1. This source is invisible in optical wavelengths, but was discovered through its centimeter radio emission. A well-defined bow shock shape is seen on the HH 1 side of the central source, whereas HH 2 could be better described as broader with more substructure (see Appendix). Herbig & Jones (1981) showed that the two HH objects are moving at supersonic velocities away from their source. Tightly packed knots in HH 1 form a jet close to the generating source. The increasing observational evidence from this set of objects and others led to the notion that HH objects/shocks are formed where ejecta collide at high speeds with slower moving or surrounding material. Therefore, the spatial distribution of HH objects offers clues as to the outflow orientation with respect to the driving source, as well as mass loss and accretion history of their associated YSOs.

1.3.2. Infrared Outflows

Shock-excited outflow features are detected in both optical (HH object) and IR wavelengths. In the near to mid-IR range the emission is from molecular hydrogen ro-vibrational lines. These lines are better probes than their optical HH counterparts, for features in regions of higher extinction, and they also trace low-excitation, shocked molecular gas at lower velocities (10 to 50 km s^{-1}). Recent near and mid-infrared surveys also provide a suite of information about outflows, where the most useful probe is that of H_2 (Davis et al. 2008). In that work, emission from molecular hydrogen transitions (2.122 μm) in star forming regions of the Perseus molecular cloud was observed, and many shock-excited knotty outflow features (H_2 knots) were seen. Davis, Scholz, Lucas, Smith, & Adamson (2008) noticed that the knotty H_2 features were confined to a small region of the flow area, whereas the bow shock emission features occur at the outer edges of the CO flow lobes (see next section).

The main goal of this thesis is to identify and ultimately characterize the outflows we find when looking through infrared maps of molecular clouds in order to further understand this crucial phase of star formation. We must then answer the question: what do outflows look like in *Spitzer* bands from 3.6 to 8.0 μm? From early releases of *Spitzer* data, outflows from young stars could be seen as diffuse emission knots, brightest in the 4.5-μm band, as expected for dominating shocked H_2 emission. And, although the *Spitzer* bands are not as sensitive to outflow emission as 2.12 μm H_2 survey maps (Walawender et al. 2005; Davis et al. 2008), the outflow features are clearly observed indicating that a survey conducted with these particular near-infrared bands is a viable method for identifying outflows. In Sect. 3 I present our search for these *Spitzer* outflow features using data from the SST IR bands, from 3.6 to 8.0 μm. The bands effectively cover the pure rotational H_2 lines S(0)–S(7) between 5 and 30 μm.

1.3.3. Molecular Outflows

Outflows are also detected through observations of molecular rotational line transitions at millimeter and submillimeter wavelengths, giving rise to the name molecular outflow. In the 1970s astronomers saw that CO emission lines were broader than expected inside molecular clouds. This excess in radial velocity, seen as expanded widths from Doppler shifts, with both red and blue shifted sides, or "wings," indicated that two lobes were moving in opposite directions. As before, it has since been established that for the most part, observations in this wavelength range trace the cloud gas that has been entrained by the underlying protostellar wind (as seen in Fig. 5b).

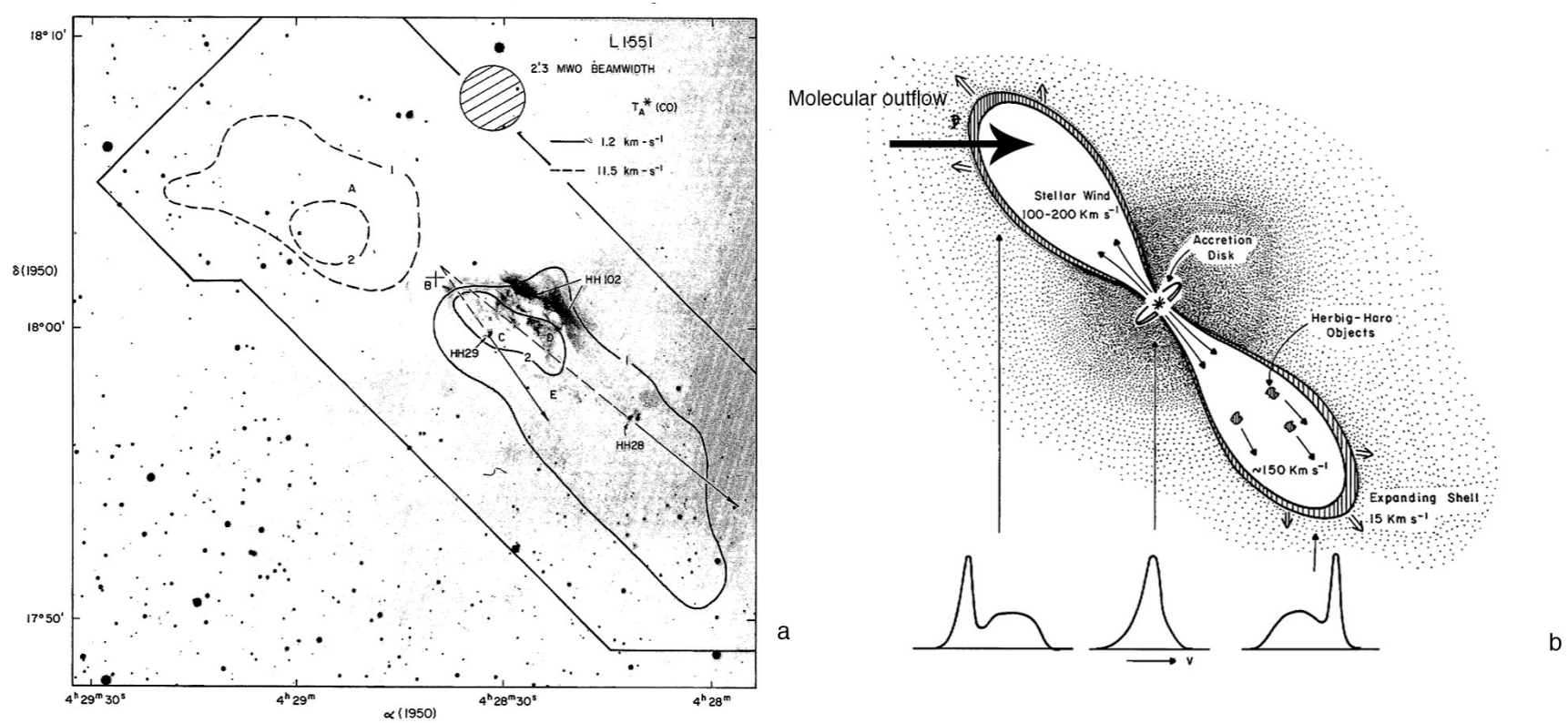

Fig. 5.— The overlap of molecular outflow in CO and HH objects is evidence that these two phenomena are related. **a** Contour map of L1551-IRS5 made from spectra of carbon monoxide ^{12}CO (J = 1–0), superimposed on an optical image of Herbig-Haro objects HH 28, HH 29, HH 102. **b** Schematic picture of an outflow in a stellar wind model, with line profiles for areas of outflow activity at different distances from source shown at *bottom*. Both figures from Snell et al. (1980)

Again as an example we examine the first object of this kind to be discovered and mapped, L1551-IRS5 (Fig. 5a), in the L1551 dark cloud, part of the larger Taurus-Auriga cloud complex (see Fig. 1). Snell, Loren, & Plambeck (1980) showed that the axis of the blue-shifted CO lobe seen in L1551-IRS5 spectra, coincided with the direction of the proper motions of HH 28 and HH 29, which also had blue-shifted radial velocities (Fig. 5b). This evidence proved that the CO molecular outflow was indeed related to the HH objects in some way. Subsequent surveys of gas around YSOs also revealed that bipolar CO outflows are a common feature in low-mass ($< 1\ M_{\odot}$) protostellar systems, with typical lengths on the order of 1 pc (Bally & Lada 1983). Figure 5a aims to show how the two manifestations of outflow phenomena overlap, by plotting the contours made from CO data at radio wavelengths over an optical image of HH objects of the same region.

1.4. Importance of Outflows and This Work

Outflows are important to the star formation process in many ways. For instance, they are a product of the transfer of angular momentum from the accretion disk onto the forming star, which would otherwise break apart the protostellar system (Hartmann & MacGregor 1982). Outflows also stop the accreting process by clearing out envelope material surrounding the protostar, effectively reducing the infalling material so that no more is accreted onto the disk-star system (Velusamy & Langer 1998). From Reipurth, we can imagine HH objects, or more generally outflow knots, as a "fossil record" of mass loss and mass accretion in the formation of a star. The outflow symmetries that result from this mass loss provide clues about the nature of the engine, and provide more constraints on models of star formation. All these issues illuminate how the protostar interacts with its natal cloud, and may provide a more complete picture of stellar evolution.

The work presented here is an attempt to create an extensive and accurate survey of outflows in nearby star forming regions. Since we have such a large data set consisting of over, the comparison between outflows and their sources will be both homogenous and comprehensive. Earlier work studying molecular clouds observed by *Spitzer* have merely mentioned the occurrence of outflows, but did not provide much quantitative information. Our analysis determines the abundance of outflows in these regions, outflow areas, and lengths, among other observational properties.

In addition, by taking advantage of Spitzer's particular sensitivity to both outflow and source emission wavelengths, we also aim to find relationships between protostellar and outflow properties. In terms of these relationships, we expect to see higher luminosity objects having more outflows associated with them. We also expect to see some trends in how the lengths of outflows depend on YSO class. Another trend we predict is that these protostars will be Class 0 or I sources, which means they would be cool and more red than other classes of YSOs.

2. Observations and Data Reduction

2.1. Spitzer Space Telescope

The *Spitzer Space Telescope* (SST) was launched on August 25, 2003, into a heliocentric orbit, trailing the Earth. Named after Dr. Lyman Spitzer, Jr., the first to propose telescopes in space, *Spitzer* is part of NASA's Great Observatories Program, including the *Hubble Space Telescope*, which is a group of four orbiting observatories, each observing the Universe in a different wavelength regime. Where the Hubble observes in the visible, *Spitzer* is a telescope that observes objects in space in infrared bands. During its lifetime, *Spitzer* has obtained images and spectra from the near to far-infrared, from 3.6 to 180 μm, where almost all of this radiation is blocked by the Earth's atmosphere and since, cannot be observed from the ground.

The SST is a 0.85-meter telescope with three cryogenically-cooled science instruments: the Infrared Array Camera (IRAC), Multiband Imaging Photometer for Spitzer (MIPS), and the Infrared Spectrograph (IRS). The observations used in this work were obtained with IRAC and MIPS instruments, and the data processed by the c2d *Spitzer* Legacy Program. The instruments are well-described in Fazio and Reike (see Sect. 2.2). IRAC observes at 3.6, 4.5, 5.8, and 8.0 μm, its four wavelength channels, simultaneously, where each detector array is 256 $\times$ 256 pixels in size. Each pixel covers 1.2 arcsec, providing a 5.12 $\times$ 5.12 arcmin field of view (these are later mosaicked by c2d). In the short wavelength pair (3.6 and 4.5 μm) indium antimonide (InSb) detector technology is used, and in the long wavelength pair (5.8 and 8.0 μm) arsenic-doped silicon impurity band conduction technology (Si:As IBC) is used.

MIPS is comprised of three detector arrays in the far infrared, designed to provide deep imaging at 24, 70, and 160 μm, and measurements of spectral energy distributions between 52 and 100 μm. The first band at 24 μm is a 128 $\times$ 128 arsenic-doped silicon (Si:As) array, with a 5 arcmin field of view; the second is a 32 $\times$ 32 gallium-doped germanium (Ge:Ga) array at 70 μm for a 5 arcmin field; the third band is centered at 160 μm a 2 $\times$ 20 Ge:Ga array, mechanically stressed to extend its photoconductive response to 200 microns, with a field of 0.5 $\times$ 5 arcmin. We use IRAC and MIPS images to study outflows in molecular clouds, where the MIPS data is sensitive to the young stars and IRAC bands are sensitive to the outflow nebulosity.

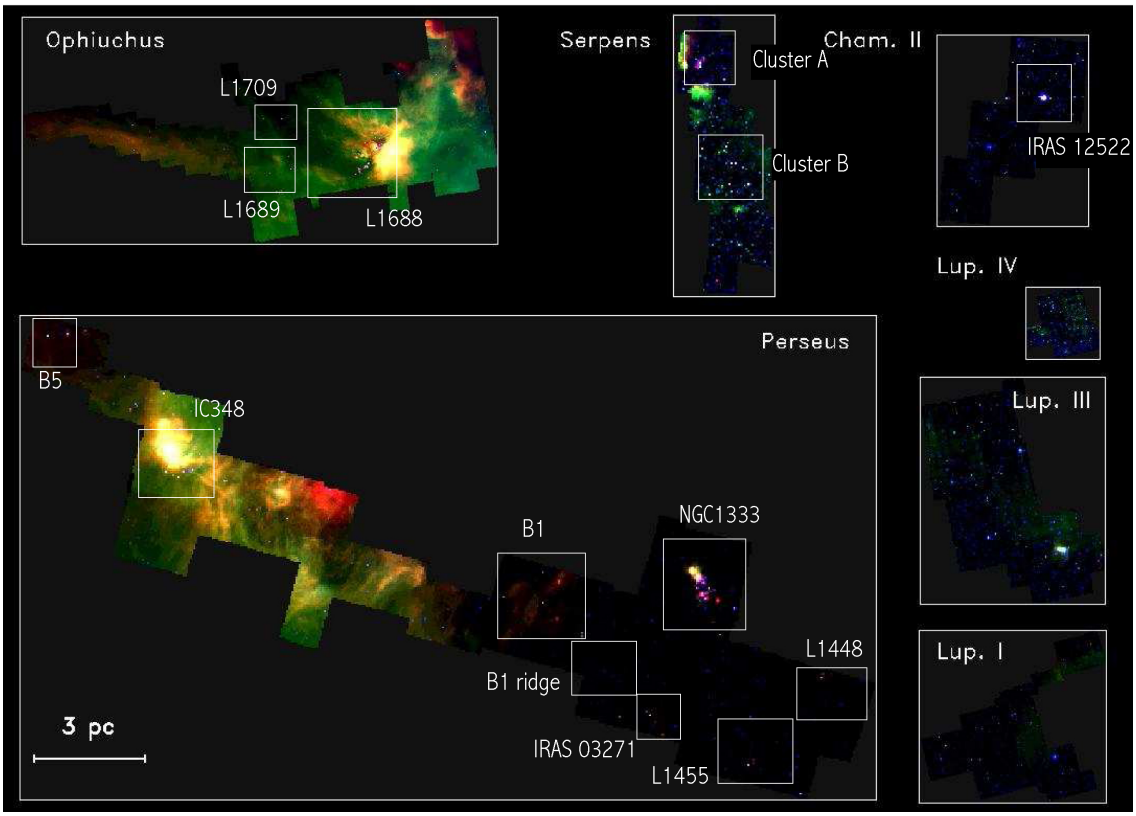

Fig. 6.— Color composite images of the five nearby ($d \leq 300$ pc) parsec-scale molecular cloud complexes observed by c2d, taken with the instruments aboard the *Spitzer Space Telescope*. The blue is 4.5 μm (IRAC band 1), green is 8.0 μm (IRAC band 4), and red is 24 μm (MIPS band 1). The clouds are shown to scale. From Evans et al. (2008)

Table 1. Basic properties of the five c2d molecular clouds. The area refers to both IRAC and MIPS data. From Evans et al. (2008) and references therein

Cloud	Distance [pc]	Area [pc^2]	Mass[a] $M_\odot$	Number of YSO
Cha II	178 ± 18	10.0 ± 2.0	595 ± 120	26
Lupus[b]	150 ± 20	28.4 ± 6.5	1138 ± 262	94
Perseus	250 ± 50	73.6 ± 29.4	6724 ± 2690	385
Serpens	260 ± 10	17.5 ± 1.4	2815 ± 217	238
Ophiuchus	125 ± 25	31.4 ± 12.6	3048 ± 1219	292

[a]The masses are calculated from extinction maps, as described in Evans et al. (2008).

[b]The Lupus clouds I, III and IV are summed for presented values.

2.2. From Molecular Cores to Planet-Forming Disks

We use both the IRAC and MIPS observations obtained by the *Spitzer* Legacy program "From Molecular Cores to Planet-Forming Disks" (c2d henceforth). The work in Evans et al. (2007) provides a complete description of source extraction and band-merging processes of these images. Data from IRAC bands 1, 2, 3, and 4, along with MIPS bands were obtained by us directly from the c2d archive (http://ssc.spitzer.caltech.edu/legacy/). The c2d program set out to provide unbiased infrared maps from 3.6 to 70 μm, of five nearby large cloud complexes in our galaxy, plus about 90 isolated dense molecular cores, in order to have a homogeneous method of studying the evolutionary sequence from dense cores in molecular clouds to stars forming with circumstellar disks. These maps are accompanied by 2MASS (Two Micron All Sky Survey) archival data and ground-based (sub)millimeter observations to effectively cover the spectral range in which young stars emit, from 1.24 μm to 1 mm. This broad wavelength range allows for a better determination of SEDs of the young stellar sources.

The five cloud complexes are shown in Fig. 6 and are: Serpens, Perseus, Ophiuchus, Lupus (I, III, and IV),[d] and Chamaeleon II. These were chosen since they covered a wide range of already known regions of star formation and are discussed individually in the following, among others: Serpens (Harvey et al. 2007); Perseus (Jørgensen et al. 2006); Ophiuchus (Padgett et al. 2008); Lupus (Merín et al. 2008); Cha II (Alcalá et al. 2008). Evans et al. (2007) describe the method of identifying YSO candidates from the *Spitzer* data and how the SEDs for each of these candidates were compiled. We use a subsample of the full catalog of c2d sources, as determined by a number of criteria, in our search strategy as a first impression of stellar content in the clouds and call these "MIPS sources." We are also of course interested in the YSO content, since these are the usual suspects that drive outflows, but this subset of sources was not used in our outflow searching scheme so that we could have an independent identification of YSO candidates where possible. Sources were traditionally selected as YSO candidates by c2d if they had an excess in near-infrared to far-infrared emission. That is, if they had rising fluxes from short to long wavelengths and high infrared luminosities, calculated over the 2MASS and *Spitzer* bands, from 1.25 to 70 μm. The resulting stellar properties from the c2d catalog of sources are used in later analysis steps (Sect. 4.2.2) where we discuss the YSO content in each of the molecular clouds (personal communication, M. Dunham, 2008). Table 1 provides basic properties of the five clouds, including the number of young stellar object candidates found by the various authors, as given by Evans et al. (2008). Due to technical reasons that the MIPS scan length can only be chosen from a fixed list, the regions observed by MIPS are larger than the IRAC observed areas, where MIPS regions are a factor of 2 to 3 larger. The sizes given for the clouds take this into account and are calculated from the IRAC observations.

[d]For simplicity we will from here on refer to these regions of the Lupus cloud complex as "Lupus".

3. Outflow Identification Method

Here I describe our method for identifying outflows. I discuss the search (Sects. 3.1 to 3.3) and how I trace the subsequent markup to form outflow lobes (Sect. 3.4), and also how we associate these lobes with sources (Sect. 3.5). To the best of our knowledge, only one other attempt has been made to examine *Spitzer* IRAC images by eye with the purpose of cataloging nebulous knots (personal communication, Stapelfeldt 2008). There they examined the Taurus molecular cloud for shocked regions as part of the *Spitzer/Taurus Legacy Survey*. We developed our own strategy into a systematic method for identifying outflows and their sources by visual inspection. The following explains how we defined outflow nebulosity, and the steps we took to then clump this together to form lobes of an outflow. The search was conducted by visually examining the five cloud complexes in the c2d data, looking at each cloud in IRAC bands 1, 2, 3 and 4 (3.6, 4.5, 5.8 and 8.0 μ m) independently, to either confirm or deny that an object exists and is of interest. The task here was to develop a search method that was consistent and therefore easily reproducible. All visual inspection was performed using the imaging application SAOImage DS9 (developed by Smithsonian Astrophysical Observatory, http://hea-www.harvard.edu/RD/ds9/).

3.1. Feature Definition

Our primary goal was to identify outflow activity in the clouds, but we first had to examine how this appeared in *Spitzer* images. So as an initial step, we looked through the images in order to find systematic definitions of objects we intuitively started to organize into categories. The result from this are the definitions displayed in Table 2. From here, we assumed that candidate outflow nebulosity was characterized as containing knot-like features. Knots are defined as irregularly shaped extended objects, with diameters of less than 10 arcsec, measured along their shortest axis. In other words, I looked for filamentous structures with a bright compact region. These knots are often found in groups or chains. We also visually searched for candidate young stellar objects (YSO) that may drive outflows in these regions. YSO candidates are first spotted as MIPS sources with nebulosity significantly brighter than background levels, which is seen when varying the intensity of the image. We also spot sources that are immediately associated with elongated emission within 5 arcsec, and are identified by searching for objects that are circular at high intensities, but have a monotonically increasing elongation when going to lower intensity levels. It is worth noting that we do not initially use the YSO source lists from c2d in this first step, as we aim to independently identify our own set of YSO candidates, which may or may not be included in the published c2d lists.

Table 2. Definitions of search categories

Category	Physical definition	Observational definition
	Active search	
Outflow nebulosity	Nebulosity due to YSO outflow activity	Extended features that contain "knots" (smaller than 10 arcsec along their shortest axis) that are detected in at least 2 bands
YSO with outflow base	YSO with outflow nebulosity	MIPS source to which nebulosity forms an elongation emerging from its immediate envelope
YSO with nebulosity	YSO with nearby outflow nebulosity	MIPS source apparently associated with nearby nebulosity
YSO with disk	YSO accretion disk seen as a silhouette	Sharp gaps between outflow nebulosity and the apparently driving MIPS source
Shell	Excavations blown into a cloud by some YSO	Near-circular structures centered on some MIPS source
Interesting	Any interesting structures not captured by other categories	No particular rules
	Passive search	
Galaxy	Background galaxies in the images	Sources of obvious extragalactic nature (e.g., spiral galaxies), and compact (of order 10 arcsec) features of "regular" shape (i.e., circular symmetric or elliptic)
Artifact	Imaging artifact without celestial counterpart	Obvious artifacts (e.g., diffraction patterns), and nebula-like features that are seen in only a single band

Table 2 describes the three categories of YSO candidates that we search for, keeping in mind that these designations are only used by us to later characterize the suspected outflow source. The remaining categories in Table 2 are physical and observational definitions of additional objects we actively search for in the images such as shells and other interesting objects, as well as structures noted in passing, such as galaxies or artifacts. Galaxies are identified as extended nebulosities with a somewhat symmetric shape, whereas artifacts can appear as many things, from comb-like features, to fuzzy diffraction spikes around bright sources. We also emphasize that not all galaxies and artifacts are found in the images, just those that are noticed and/or may be confused with outflow nebulosity in later analysis steps. Figure 19 (flow diagram in Appendix) shows this first step of feature identification, with later steps detailing the iteration process of examining the same area in multiple images.

A Note on Guiding Principles

It may be the case due to human error that a fuzzy or knotty object is occasionally missed. Since we expect outflows to be a series of knots and not just one lone extended structure, then this is acceptable and does not detract from our results, but in fact ensures that our observations are robust. We also recognize that a certain amount of personal calibration occurs while going through the images, meaning that once a person has tuned his/her eye to look for certain limits of outflow nebulosity, then that sensitivity is carried through all iterations of the search and is therefore consistent.

3.2. Visual Examination of IRAC2 Map

With the search definitions of the objects in place, the following describes the actual search procedure. Outflow nebulosity has a higher contrast in IRAC2 than in the 3.6, 5.8, or 8.0 μm bands, and thus I begin the search there. A sea of cyan-colored circles was applied before searching, which represents sources detected by MIPS, and is a first sample of potential YSOs. Following the process from Step 1 in Fig. 19, I systematically searched band 2 and marked the objects found with different colored circles, where color indicates type of object (see Fig. 7). Again, our primary goal was to identify outflows, which we decided is characterized as containing knots. At this point, I circled the positions of the knots, where the diameter of the circle indicates the size of the feature, defined as the maximum scale beyond which a knot melts into the background. When many knot-like features appeared to be related, and were separated by gaps smaller than the individual features, we said these features formed a group and marked them with single circle. If the region was crowded and a circle could not efficiently contain only those objects within a group, then a group's extent was indicated by a line spanning across the individual parts to still show that these objects were related. Circles were not allowed to overlap, so that in the later steps of analysis we could more easily characterize the areas of outflow nebulosity.

The second category of objects we were most interested in identifying was YSO candidates. These are circled in magenta, and according to the observational definition, they may be associated with a cyan MIPS source and have some elongated emission surrounding it. This mark-up served as input for later association of outflows to their sources (see Sect. 3.5). Other objects were marked, namely shells in white, and interesting objects that did not fall into the outflow, artifact, or galaxy categories, marked in blue. Candidate artifacts were marked in red and candidate galaxies in yellow, where as before, both these are marked in order to distinguish them from true outflow nebulosity. Shells are described in Table 2 as blown out cavities from a young source. The "interesting" category has an even broader definition, in that any reflection nebulae or peculiar object that does not satisfy the other categories, gets placed here for later inspection. Experience shows that nearly all the outflow nebulosity ($> 90\%$) in the cloud is identified in this first pass of examining the field.

3.3. Searching Remaining IRAC Maps

In this step, I examined each remaining IRAC band independently, carrying the mark-up over from previous steps, in order to confirm the circled objects (we only require outflow nebulosity, galaxies and artifacts to be confirmed). This step has two parts: (i) compare already marked objects from IRAC2 with next band, (ii) look for new nebulosity. For the first part, I checked for counterparts of knots detected in IRAC2 in the IRAC1 (3.6 μm) band. If circled IRAC2 nebulosity was again seen in IRAC1 then this is *confirmed outflow nebulosity*, and a box was placed around it (Step 2, top right of Fig. 7). If the structure was not seen in this second pass of the cloud, then I moved this to the artifact category, documenting this change in category (see Step 2 of flow diagram in Appendix). This newly moved object will again be checked to see if it is detected in the forthcoming bands.

Next, I checked if IRAC2 candidate artifacts appear in IRAC1. If they do, then these structures are moved from the *candidate artifact* category to the *confirmed nebulosity* category, since they are seen in at least two images and can therefore be confirmed as real.[e] If the IRAC2 candidate artifacts did not appear in IRAC1, then it was left as a candidate artifact until it marked as a confirmed artifact in later passes, having appeared in only one image and thus according to our definition, not a real structure. The same procedure was used for candidate galaxies, where if I see the same regular structure in IRAC1 as in IRAC2, I confirmed this object as a galaxy. If it did not pass the criteria for a galaxy, then the structure was moved to confirmed outflow nebulosity, since it is seen in more than one band. The various paths an object can take in this image comparison process is shown graphically in Figs. 19 and 20 in the Appendix.

[e]I conducted the search in this way due to the fact that artifacts appeared in different locations in different bands, so we had to take care not to include them in our outflow knot category.

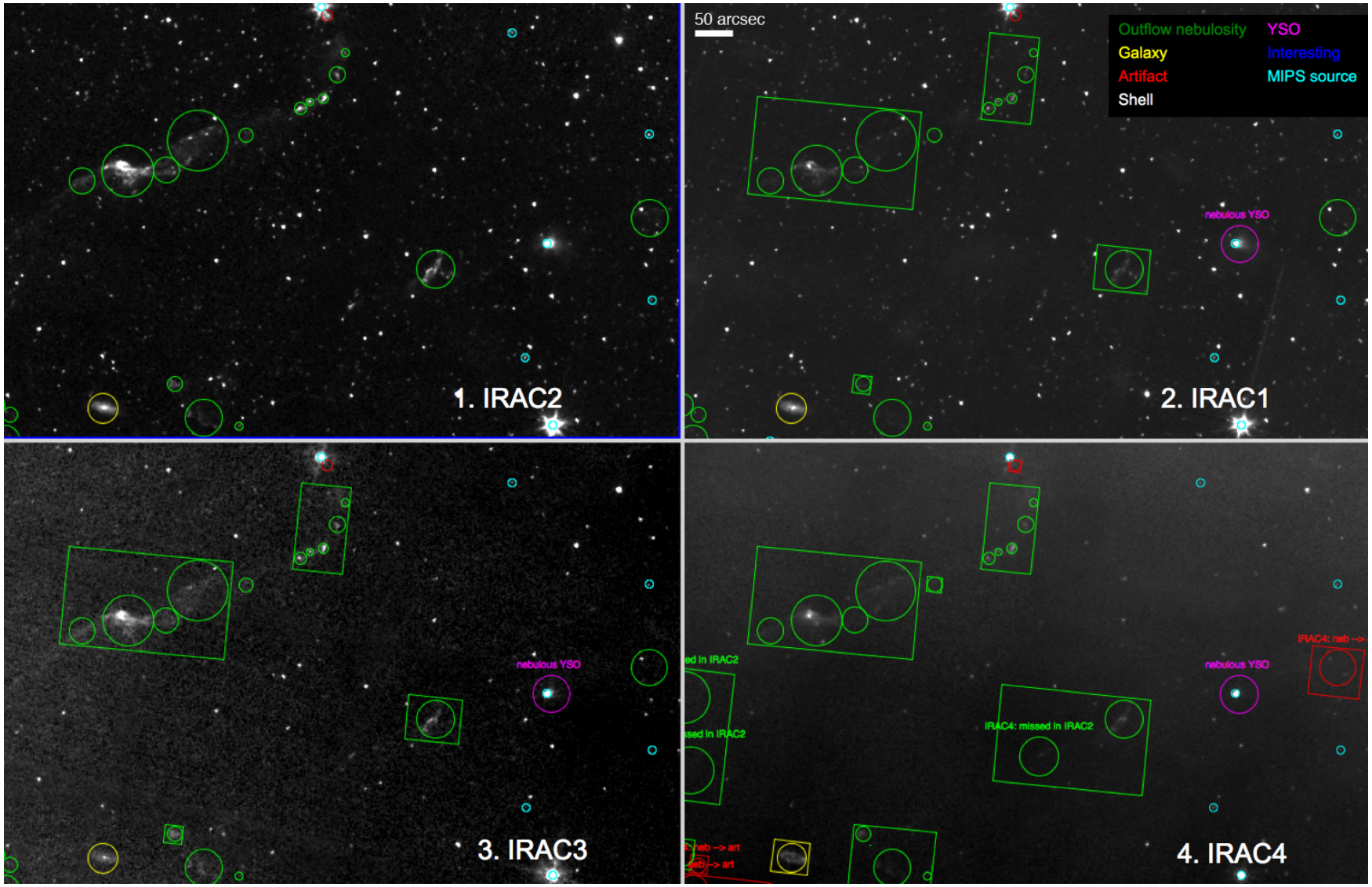

Fig. 7.— Four stages of search in L1455 of Perseus: (1) IRAC2 at 4.5 μm, (2) IRAC1 at 3.6 μm, (3) IRAC3 at 5.8 μm, (4) IRAC4 at 8.0 μm. The color code for objects is shown in the upper right corner, where green is outflow nebulosity. One can see the progression of mark-up for example in the far left collection of knotty objects. They are first detected at 4.5 μm, then confirmed in 3.6 μm

Second, I searched unmarked areas for new nebulosity or nebulosity missed in the inspection of band 2. Candidate nebulosity seen first in band 1 was marked, and the wavelength at which it was initially detected was registered. This nebulosity was immediately checked by comparing to band 2, but left as a candidate to be confirmed in further bands if not confirmed right away. If the structure was not initially detected in band 2, though it was obviously there, I noted that I missed it in the first pass (i.e., not a usual IRAC2 detection, but indicate it was missed before). I also take into account the fact that different IRAC bands cover slightly different regions of the clouds by noting if any objects were affected by this discrepancy. Candidate YSOs marked in band 2 did not need to be confirmed in band 1, but any new sources noticed to exhibit candidate YSO characteristics were marked and included in the candidate YSO category. After the IRAC1 band was inspected, I repeated the process for the IRAC3 and IRAC4 bands. At the end of the search, different generations of mark-up culminated into a final version of the mark-up in the last stage of examining the IRAC4 band, as seen in Fig. 7.

3.4. Tracing of Outflow Lobes

At this point in the outflow identification process, we have a final version of the mark-up after independently examining the four IRAC bands. From this I divided the clouds into regions for organizational purposes, either using known cores as a reference or by another name (for regions in Perseus and other clouds see Table 4). Next, knots were organized into coherent outflow lobes. The initial tracing was done manually by going through the IRAC2 image with the final mark-up displayed, and placing a polygon (shape option in DS9) around groups of outflow nebulosity that intuitively appeared to be related, starting from the outer-most nebulosity all the way to the suspected driving source, where possible. There were cases where IRAC knots were seen at far distances from well-traced lobes, and so were added as an extension to a lobe that included close-in knots. These extensions do not include the source. In other cases, the driver is unknown and therefore not included in the outline of the lobe. Figure 8 is an example of our tracing scheme where outflow nebulosity delineates the outflow shape, and the extension type of lobe is shown as well (in yellow). This initial tracing was first performed on a qualitative basis, but we quantify the certainty of the lobes by evaluating each with the following criteria:

1. *Is the lobe well-sampled with outflow nebulosity?* In this case, outflow nebulosity can also refer to low-level emission that did not qualify as knots, and therefore not circled in the original mark-up, but obviously belongs to the outflow system and extends to connect knots (seen as diffuse emission in top lobe in Fig. 8). A quick measure of a lobe being "well-sampled" is if the largest distance between outflow nebulosity is shorter than 1/3 the total lobe length, then we say this lobe is well-sampled and receives a positive rating ("Y" for "yes" in column 1 of Table 3). On the other hand, if the lobe is only loosely populated with knots, and no or very little faint emission is seen, this lobe would receive a negative score ("N" for "no"). Table 11 shows the criteria evaluated for each lobe traced in all c2d clouds, where Table 3 only shows a few cases.

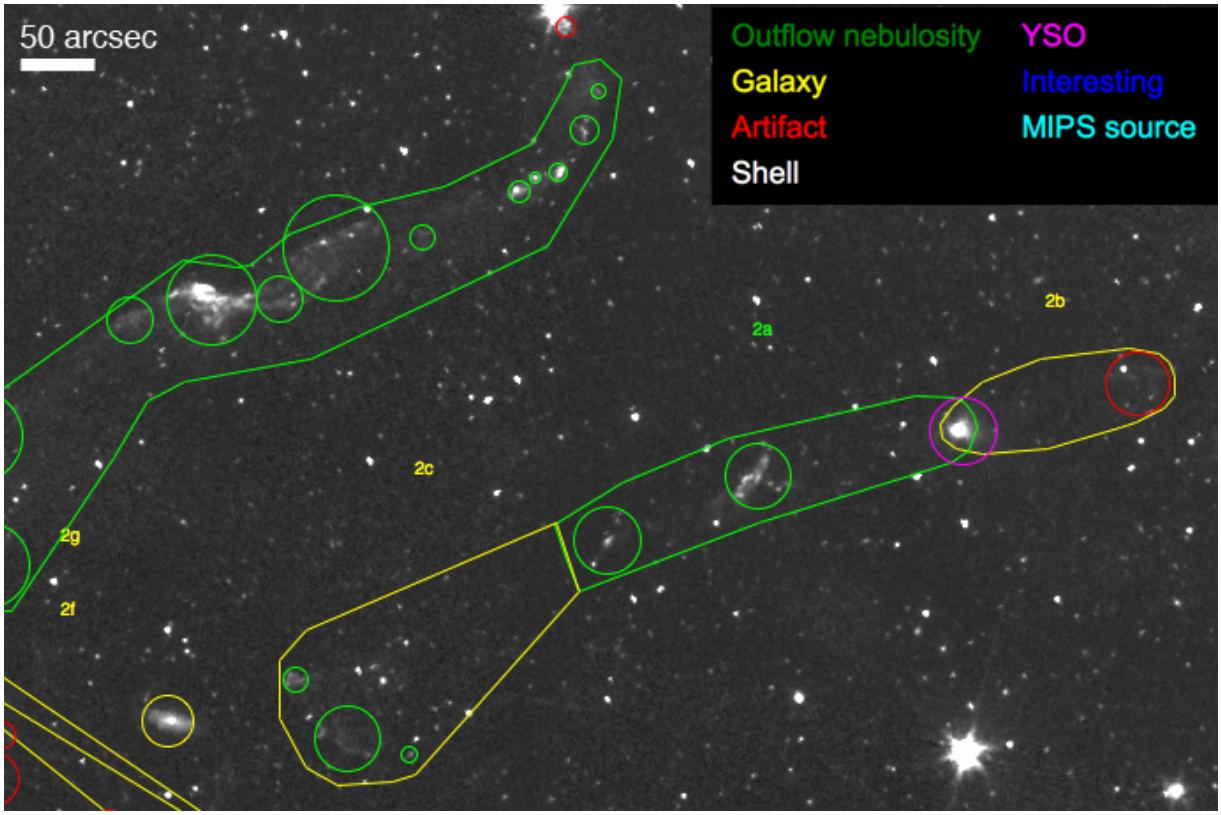

Fig. 8.— Tracing example in L1455 (same region as in Fig. 7). We see in the *top* lobe that many circled IRAC knots indicate the shape of the outflow. The bottom lobe, labeled 2a (naming scheme described below), contains fewer knots but they are included in one lobe since there were no other knots in the immediate area and the suspected source seemed to be extended. The yellow lobe 2c, extending from 2a, contains knots that lie further out but still seem to be associated with the 2a lobe, thus I draw it as an extension

2. *Is the outflow nebulosity in a non-confused region?* The lobe passes this criteria if the outflow nebulosity included in the traced lobe is isolated in some way from other circled nebulosity, i.e., it is clear that a group of knots included in the lobe do not belong to another outflow lobe. There is the obvious case of B5, where we circle only two lobes of an outflow in a region that is not crowded with many outflow knots (Fig. 9).

3. *Is there a signature bow shock shape?* Sometimes the shape of the knots indicate the flow direction. This is most apparent with V-shaped and C-shaped groups of knots, known as bow shocks from outflow models. If these structures are observed when tracing a lobe and they point back to the source, then the lobe receives a "Y" rating. This criterion is used mainly to include those lobes which are very long and thus not so well-sampled, but we are still certain that the lobe exists in this form.

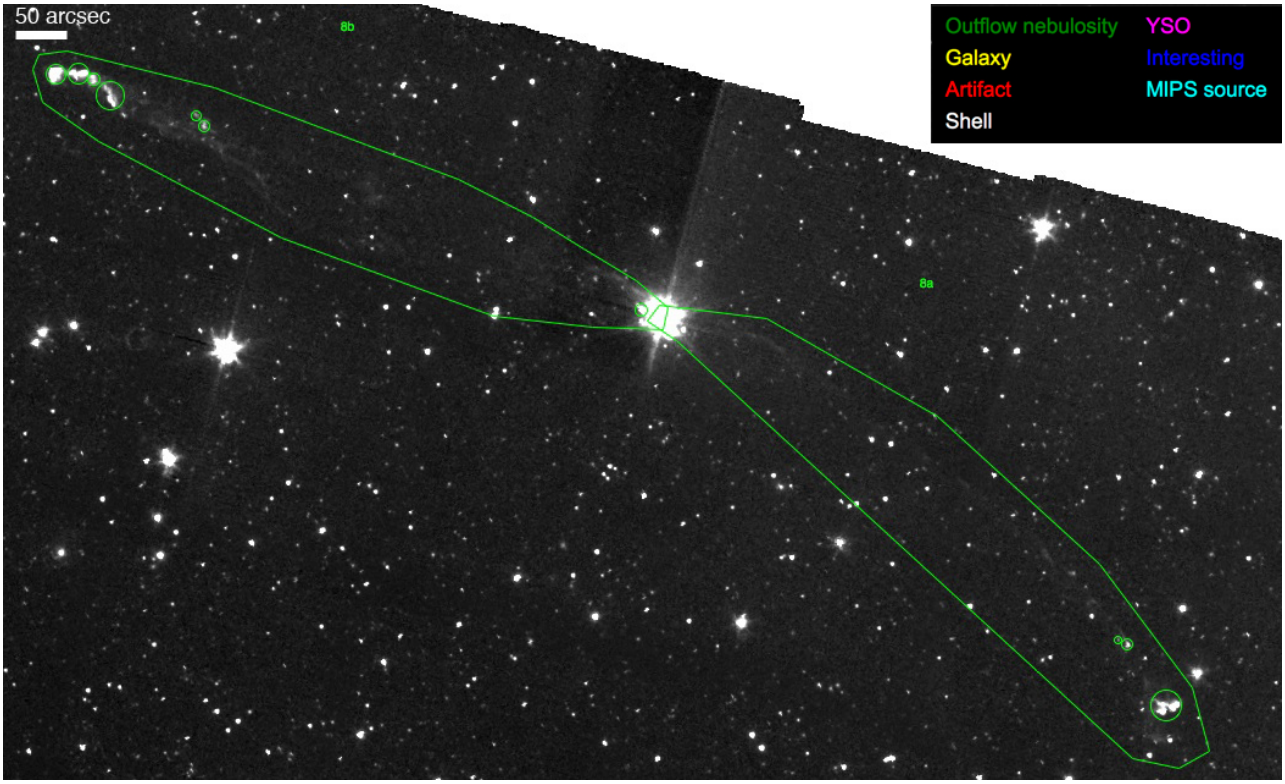

Fig. 9.— Case (i): A class lobes in B5 (IRAC2). (**a**) Low-level emission that extends from source to knotty features in upper left and lower right corners. (**b**) Both lobes are class A because they are well-sampled and outflow nebulosity is in a non-confused region

We organize the lobes into three categories: either certain (A), possible (B), or unclear (C) (seen in last column of Tables 3 and 11), according to their scores from the above criteria. Table 11 gives the ratings of the lobes for all 86 lobes found in this survey, where the naming scheme is given by cloud name (Per-), then region number in that cloud, and order of lobe, e.g., the first lobe in the first region in Perseus is Per-1a. Lobes can be classified as A class if (i) it scores Y in the first and second column, or (ii) it scores Y in the second and third column. Referring to case (i), we take lobes in B5 as an example (Fig. 9). Here, few knots are circled, but there is low-level filamentary emission spanning the distance between the suspected source and the outlying knots, therefore the lobes receive a positive score in the well-sampled test (Y in col 1). Looking at a zoomed out image (Fig. 10), that these two lobes in B5 are indeed in a non-confused region (Y in col 2). Positive scores in the first two columns qualifies these outflow lobes for class A designation. For case (ii), lobe Per-1i provides an excellent example, where we see it is not well sampled (N in col 1), but is in a non-confused region (Y in col 2), and has a signature bow shock shape (Y in col 3); therefore, it is an A class lobe. If these two configurations (i or ii) are not satisfied, then we say the lobe is either a B or C class lobe.

The B class designation is for lobes which are in a confused region (N score in col 2), and are either not well-sampled or do not possess a bow shock shape. For the case where we are certain that a lobe exists (A class), but there is some outlying nebulosity that may or may not belong to this outflow, we call this an extension and label it as a B class lobe (see lobe Per-2c in Fig. 8). These extensions may also occur when taking into account artifacts or objects labeled as artifacts in our regime because they did not appear in at least two of the four IRAC bands. The C label is applied when nebulosity enclosed in the lobe is only loosely associated and there does not seem to be a source from which this material was ejected. This occurs very rarely as most outflow nebulosity is found in clumps and there is some idea of its source. Figures 10–13 show all lobes marked in this survey.

Table 3. Abbreviated version of Table 11 in Appendix, showing the classification scoring for a two lobes from the L1455 region in the Perseus cloud

Lobe name	Well sampled? 1	Non-confused region? 2	Bow shock shape? 3	Class
Per-2a	Y	Y	N	A
Per-2b	N	Y	N	B

3.5. Association of Outflow Lobes to Sources

We also evaluate the association of lobes with their suspected sources by inspecting the outflow environment in the IRAC images, and also using the MIPS bands to point out likely drivers. Sometimes the source of an outflow is apparent, especially in non-confused regions, and with faint emission that ostensibly traces the lobe from close to the suspected source to more distant outflow nebulosity. In other cases, the outflow source may not be clear, therefore we rank the association of lobes to sources with the following: *yes, probable, possible, unclear* and *no*.

A lobe receives a *yes* rating if outflow nebulosity, including low-level emission, can be traced directly back to a source; therefore a *yes* rating is a $definite$ association of a lobe with it's driving source, and is the highest ranking in this associating scheme. Figure 9 also provides a good example for this case, where one can connect diffuse emission from the outer knot-like features of the outflow to the source. The *probable* rating (less than certain) refers to the case where a single star is the most likely outflow generator from a closely grouped set of MIPS sources that lie roughly along the same axis as the outflow nebulosity in the lobe. The *possible* score refers to the instance where, as in the *probable* case, there is a close-packed group of drivers, but either the clustering is too dense to pick one source as the driver, or there is not much outflow nebulosity or low-level emission to act as a guide. We therefore make a "best guess" as to the driving source in this case. We also mark extensions to lobes as having a *possible* source association, since these lobes also do not have outflow nebulosity that traces back to a source or else they would have been included in their parent lobes as well. $Unclear$ represents the case where there are many sources clumped together, but unlike the above two cases, one cannot distinguish between sources at all, and/or the lobe is extended far enough away from the clustered sources that the orientation and position of the outflow nebulosity gives no clue as to the source. The *no* rating is assigned to lobes that have no clusters of MIPS sources nearby, nor much outflow nebulosity included in the lobe to act as pointers to the source.

It is important to note that this ranking of source association has no influence over the lobe classification. That is, a lobe can be marked as A class but have only a *probable* source association. Likewise, a B lobe can have a *probable* source. It is however interesting that of the 52 A type lobes, shown in Table 6, 79% (41) have a *yes* or *probable* source, whereas only 1 B lobe has a definite association (see also Table 7). This information provides a further metric for quality of lobes, where an A lobe with a *yes* source association is of the highest quality. This tells us that the two scoring regimes (classes and associations) are somewhat related, but one is not dependent on the other.

Table 4. Our adopted boundaries for different regions in clouds. The naming scheme in the last column increase with right ascension (α)

Region	Northwest corner		Southeast corner		Size	Name[a]
	α	δ	α	δ	[deg^2]	
Chamaeleon II						
IRAS12522	12:49:13.904	–76:45:37.20	12:57:39.796	–77:16:32.03	1.09	Cha-1
Lupus						
Lupus I	15:36:57.676	–33:00:42.85	15:46:48.977	–35:07:22.40	1.39	Lup-1
Lupus III	16:05:46.767	–37:36:04.97	16:15:45.618	–39:35:25.31	1.34	Lup-2
Lupus IV	15:59:10.782	–41:21:54.88	16:03:58.561	–42:15:36.33	0.37	Lup-3
Ophiuchus						
L1688	16:25:35.761	–24:05:08.14	16:29:38.527	–24:59:58.82	0.92	Oph-1
L1689	16:30:30.692	–24:20:19.86	16:33:22.330	–24:43:41.63	0.28	Oph-2
L1709	16:30:45.850	–23:53:17.44	16:32:52.022	–24:16:37.31	0.20	Oph-3
Perseus						
L1448	03:24:55.000	+30:50:26.00	03:27:15.000	+30:23:45.00	0.26	Per-1
L1455	03:26:00.000	+30:21:00.00	03:29:00.000	+29:58:00.00	0.29	Per-2
NGC1333	03:27:30.000	+31:43:30.00	03:30:30.000	+30:49:00.00	0.68	Per-3
IRAS03271	03:29:10.000	+30:37:00.00	03:32:00.000	+30:10:00.00	0.32	Per-4
B1 ridge	03:30:45.000	+30:57:30.00	03:33:10.000	+30:37:30.00	0.20	Per-5
B1	03:30:55.000	+31:27:00.00	03:34:00.000	+30:58:00.00	0.37	Per-6
IC348	03:43:25.000	+32:08:00.00	03:45:20.000	+31:54:00.00	0.11	Per-7
B5	03:46:45.000	+32:58:00.00	03:48:46.000	+32:42:00.00	0.13	Per-8
Serpens						
Cluster A	18:29:01.382	+01:29:59.14	18:30:53.041	+01:02:04.21	0.22	Ser-1
Cluster B	18:28:22.529	+00:43:50.33	18:30:00.763	+00:21:00.85	0.16	Ser-2

[a]The name we use to describe regions in analysis steps.

4. Results and Discussion

In Sect. 4.1, we begin with a description of the results from our search of IRAC images for knotty object and present Figs. 10–13, which show the outcome of this search. Lupus is not shown in this series since no lobes were found there. General properties of outflows and their sources are given in the Sect. 4.2. Then we compare outflow activity in the different clouds in Sect. 4.3, focusing on how the classes of YSOs and stellar densities play a role. Lastly, in Sect. 4.4 we describe the correlations between the physical parameters of the outflows and the YSOs that drive them.

4.1. Characterization of Cloud Regions

4.1.1. Overall Description of Search Results

Table 5 displays the number of objects described in Sect. 3.1 for each of the five molecular clouds. We detected 409 outflow knots, 6 shells, 161 other interesting objects, 87 galaxies, and 212 artifacts that were seen in only one of the IRAC bands. Even though not all of the 409 knots are included in the outflow tracings, 86 outflow lobes can be constructed from the *Spitzer* images.[f] Most strikingly we see that Perseus, the most massive of the clouds has the greatest number of knots. In Perseus alone ($\sim$4 deg^2), we detect 310 knots, where the Lupus clouds, on the other hand, make up $\sim$3 deg^2, and only have 10 detected knots. We could also construct systems of lobes about a certain source, resulting in 45 different outflow systems of one or more lobe. A large portion of these systems consisted of more than one lobe, either counterparts on the opposite side of the source or as an extension to the parent lobe. That is, 58% of the 45 are bipolar systems consisting of at least 2 lobes, and 42% had lobes on only one side of the source.

Looking to Table 6, we mark about 61% (52) as A class lobes, 37% (32) B class lobes and only 2% (2) C class lobes from a total of 86 lobes identified in the five c2d clouds. Of the 32 B lobes, $\sim$40% (13) are extensions to A class lobes, and 60% (20) are other lobes that did not satisfy the A class requirements. Table 7 shows the source association for the 86 outflow lobes. We see that 36 of 52 A lobes have a definite source association, and are thus the highest quality lobes. That is, 42% of all lobes are lobes of the highest rating, classified as both A class and with a source score 1. Accordingly, the majority (27 of 32) of B lobes have a "possible" association to a source. Again, this shows how our two rating systems are related. It is also a direct result of this that the 2 C class lobes have a "no" rating source association, the lowest class of lobes. If we do not consider lobe class, but only that a lobe has a suspected source (score "yes", "probable," and/or "possible"), then we can say that 89% (77 of 86) of all lobes have a source. For scores of all lobes found in this survey see Table 11 in the Appendix, and for a summary of outflow activity for each region in each cloud see Table 8.

---

[f]I refer to *Spitzer outflow lobes* as lobes we identified from *Spitzer Space Telescope* data and specifically characterized in this survey. Another term we should distinguish is *Class*, which we use to characterize the *Spitzer* lobes and also used to describe the spectral slope of YSOs.

Table 5. Number of objects detected in clouds

Category	Cha II	Lupus	Oph	Perseus	Serpens	All clouds
Outflow knots	6	10	51	310	32	409
Outflow lobes	1	0	16	62	7	86
YSO	3	22	11	21	8	65
Shell	0	0	3	3	0	6
Interesting	3	108	20	8	22	161
Galaxy	10	15	27	32	3	87
Artifact	11	21	54	82	44	212

Table 6. Number of lobes and their assigned class in all surveyed clouds. Under the B class, extensions and non-extensions to lobes are noted

Cloud	A class	B class		C class	Total
		Ext.	Not ext.		
Chamaeleon II	1	0	0	0	1
Lupus I, III, IV	0	0	0	0	0
Ophiuchus	10	4	2	0	16
Perseus	36	8	16	2	62
Serpens	5	1	1	0	7
All clouds	52	13	19	2	86

4.1.2. Outflow Activity in Each Region

Perseus. We now examine more closely each cloud, where Fig. 10 displays the final mark-up of regions in Perseus, with knotty objects in green. Note that since we are looking at images of objects in the sky, *western* refers to regions on the right and the *eastern* on the left. From our method (see Sect. 3) we identify 310 knot-like structures in Perseus. There are a total of 62 lobes, 58% A class, 39% B class, and 3% C class. A further subset of these A class lobes (36) are those with a definite, or "yes" source association; these make up 42% (26 of 62) of the total lobes in Perseus and are the highest rated lobes. Of the 8 dark cloud regions in Perseus, we see that the northwest area of NGC1333 contains the largest number of knots. We were reluctant here to group these knots into lobes since this is such a confused area, nevertheless we marked 15 outflow lobes in this region, around 24% of total lobes in Perseus, containing 47% of knots (146 of 310) in this cloud. The western most regions of L1448 and L1455 (Per-1, Per-2 in Table 4 lobe naming scheme) are somewhat less confused than NGC1333 (Per-3), i.e., they have fewer tighter packs of knots, with $\sim 28\%$ of the total Perseus lobes occupying this region. The central regions (IRAS03271, B1 ridge, B1) contain 23 outflow lobes, nearly 37% of the total lobes. The remaining lobes lie in the eastern portion of the cloud, which is less populated with knots, and thus fewer lobes were drawn. For example, IC348 has 5 lobes and B5 has 2 lobes, combined to make-up 11% of all Perseus lobes, with the majority being of the highest quality (A class with definite source). As we will see later, the stellar population is somewhat older than the western side (Sect. 4.2.2).

Serpens. The second cloud we examined was Serpens, and we evaluate it the same as above with Perseus. For the two regions in Serpens, called Cluster A and Cluster B by Harvey et al. (2007), we found a total of 32 knots, with 7 outflow lobes, 5 A class, 2 in B and C classes, which is merely 8% of the marked lobes in the five clouds. This low lobe number is not surprising when looking at Fig. 11, which shows the outflow activity (knots in green circles), as compared to the rest of the c2d sample. In Cluster A (Ser-1) in the northern part of Serpens lies many knots, but we were unable to confidently place many in a certain lobe, thus we mark only one outflow, albeit with an "unclear" source. We do see a higher number of artifacts than knots, which may be due to the fact that Serpens is closer to the galactic bulge and has more background stars and thus more noise.

Ophiuchus. We move to the second-most active star forming region in the c2d data, Ophiuchus (Fig. 12). We find 51 knots, which act as tracers for 16 outflow lobes (19% of total *Spitzer* lobes). Of these, 10 are A, and 6 are B lobes. All of these have either a definite YSO (score 1) as its source or some possible candidate (score 3). That is, the lobes in Ophiuchus have a more certain rating when it comes to assigning a driving source than other clouds. For reference, the scores for lobe and source certainty for all lobes can be found in Table 11. Within Ophiuchus, the majority of lobes lie in the westerly L1688 region (Oph-1). This area is dominated by bright emission from a number of clusters, and thus many knots could not be organized into specific lobes. In the eastern sections of the cloud, in regions like L1689 and L1709, the space was somewhat less cluttered and most of the knots in these regions are indeed assigned to a particular lobe.

Chamaeleon II and Lupus I, III, IV. The last two complexes we surveyed were Cham II and Lupus. We consider the Lupus clouds as one group. As we see from Fig. 13, there is very little outflow activity revealed as knots, and only 1 lobe was marked in these clouds (in Cham II). Although there is not much activity, the knots satisfied the three A class criteria, but due to the fact that they are not close-up to their source, the lobe received a "possible" rating in the source association. Examining Table 1 again, we see that Lupus and Cham II are the least massive of the molecular clouds. The lack of activity in these clouds is discussed below, as compared to other clouds which, as we will see, have a higher percentage of younger protostars.

Table 7. Association of lobe to source distributed over lobe class

Association with source	Class			Total
	A	B	C	
1 Definite (yes)	36	1	0	37
2 Probable	5	3	0	8
3 Possible	5	27	0	32
4 Unclear	6	1	0	7
5 No	0	0	2	2
Total	52	32	2	86

Table 8. Total number of c2d YSO candidates, organized by region and SED class, including YSO density. Also shown is outflow nebulosity detected, in terms of knot numbers, area and lobe numbers for each cloud region. There are a few instances where the YSOs and knots fall outside our adopted boundaries

Cloud Region	N (YSO)/ pc^2	Total YSO	Class I	Class Flat	Class II	Class III	Knots	Area (arcmin^2)	Lobes
Chamaeleon II									
IRAS12522	0.48	5	4 (80%)	1 (20%)	0 (0%)	0 (0%)	5	2.17	1
Total		5	4	1	0	0	6	2.21	1
Lupus									
Lupus I	1.36	13	2 (15%)	3 (23%)	6 (46%)	2 (15%)	3	0.19	0
Lupus III	7.51	69	2 (3%)	6 (9%)	41 (59%)	20 (29%)	4	0.17	0
Lupus IV	4.73	12	1 (8%)	1 (8%)	5 (42%)	5 (42%)	3	0.21	0
Total		94	5	10	52	27	10	0.57	0
Ophiuchus									
L1688	39.08	172	22 (13%)	37 (22%)	104 (60%)	9 (5%)	32	15.40	9
L1689	8.82	12	1 (8%)	0 (0%)	10 (83%)	1 (8%)	15	6.09	3
L1709	9.45	9	0 (0%)	5 (56%)	4 (44%)	0 (0%)	3	0.54	4
Total		193	22	42	118	10	51	22.07	16
Perseus									
L1448	1.82	6	5 (83%)	0 (0%)	0 (0%)	1 (17%)	24	20.51	9
L1455	1.79	10	5 (50%)	3 (30%)	2 (20%)	0 (0%)	35	9.28	8
NGC1333	9.35	121	41 (34%)	19 (16%)	55 (45%)	6 (5%)	146	35.77	15
IRAS03271	1.31	8	3 (38%)	1 (13%)	4 (50%)	0 (0%)	5	1.91	4
B1 ridge	2.10	8	2 (25%)	1 (13%)	5 (63%)	0 (0%)	18	15.69	6
B1	2.99	21	12 (57%)	0 (0%)	8 (38%)	1 (5%)	45	3.10	13
IC348	34.88	73	10 (14%)	5 (7%)	53 (73%)	5 (7%)	24	1.76	5
B5	1.63	4	2 (50%)	0 (0%)	2 (50%)	0 (0%)	10	0.73	2
Total		251	80	29	129	13	310	89.04	62
Serpens									
Cluster A	18.07	82	19 (23%)	13 (16%)	42 (51%)	8 (10%)	16	4.21	1
Cluster B	18.21	60	9 (15%)	8 (13%)	37 (62%)	6 (10%)	16	2.92	6
Total		142	28	21	79	14	32	7.13	7

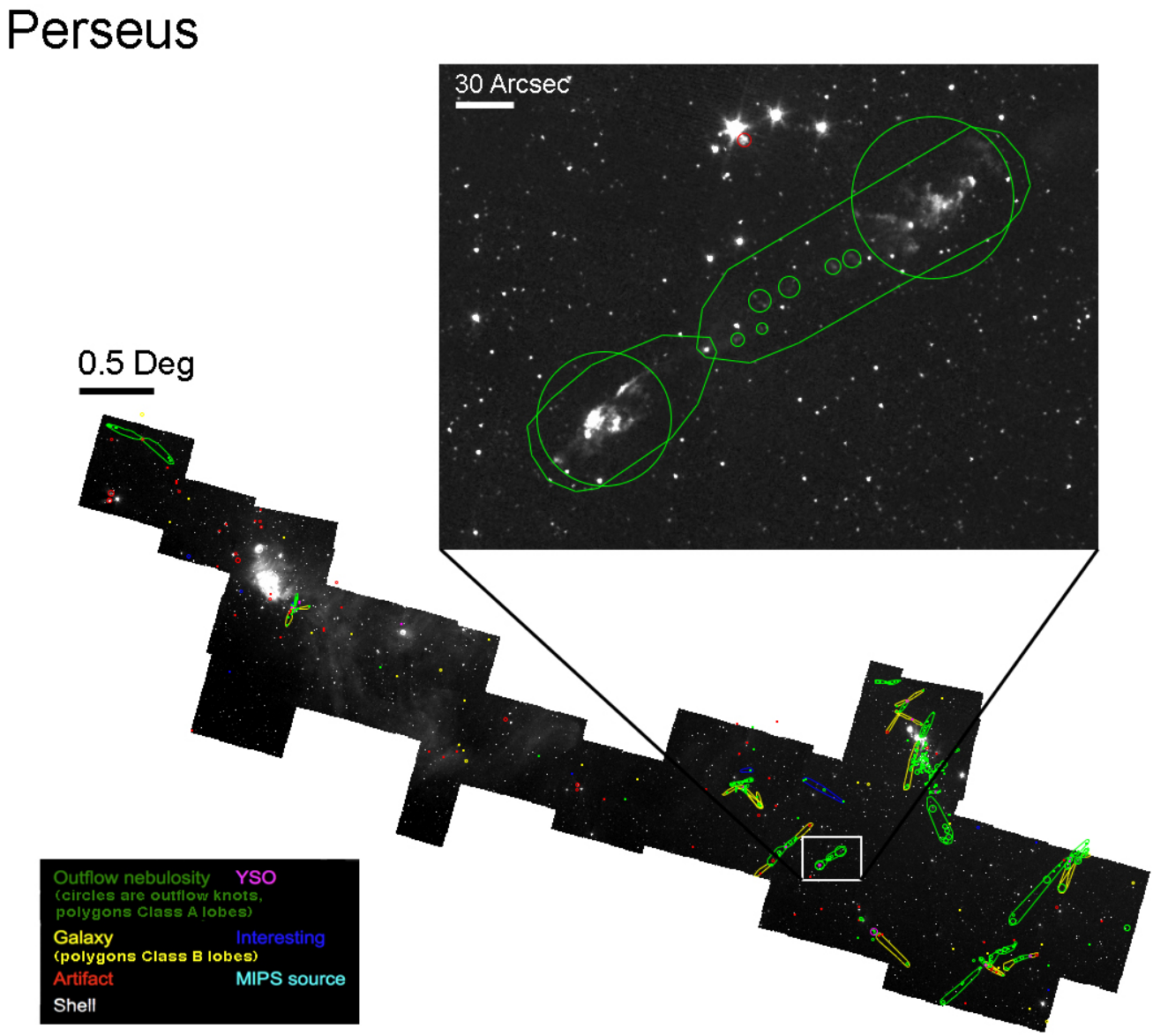

Fig. 10.— Complete mark-up from search for outflow nebulosity and lobe characterization showing the entire Perseus molecular cloud. The enlarged image in the *upper right* panel shows Per-5a and Per-5b lobes

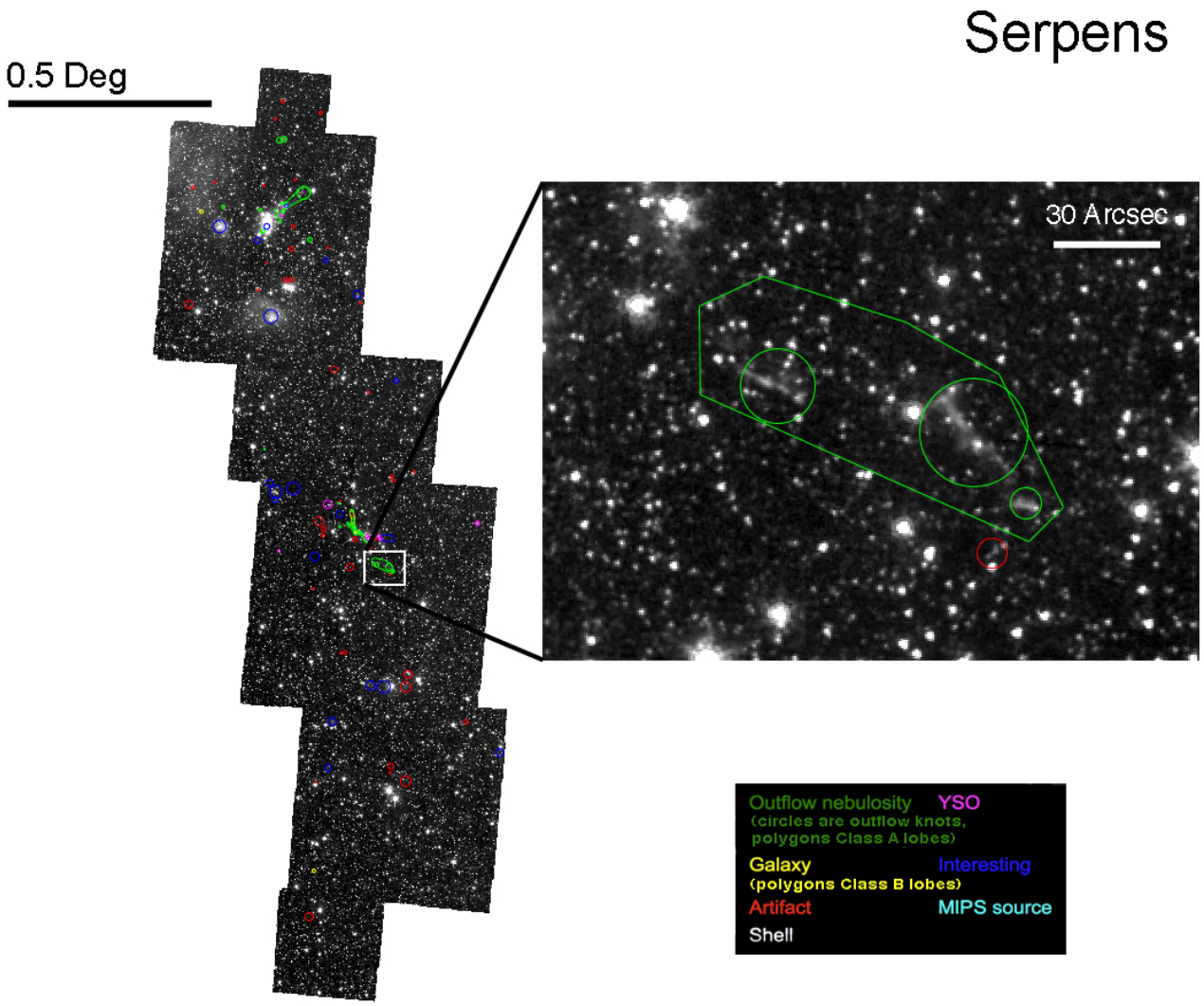

Fig. 11.— Complete mark-up from search for outflow nebulosity and lobe characterization showing the entire Serpens molecular cloud. The enlarged image in the *upper right* panel shows Ser-2a lobe

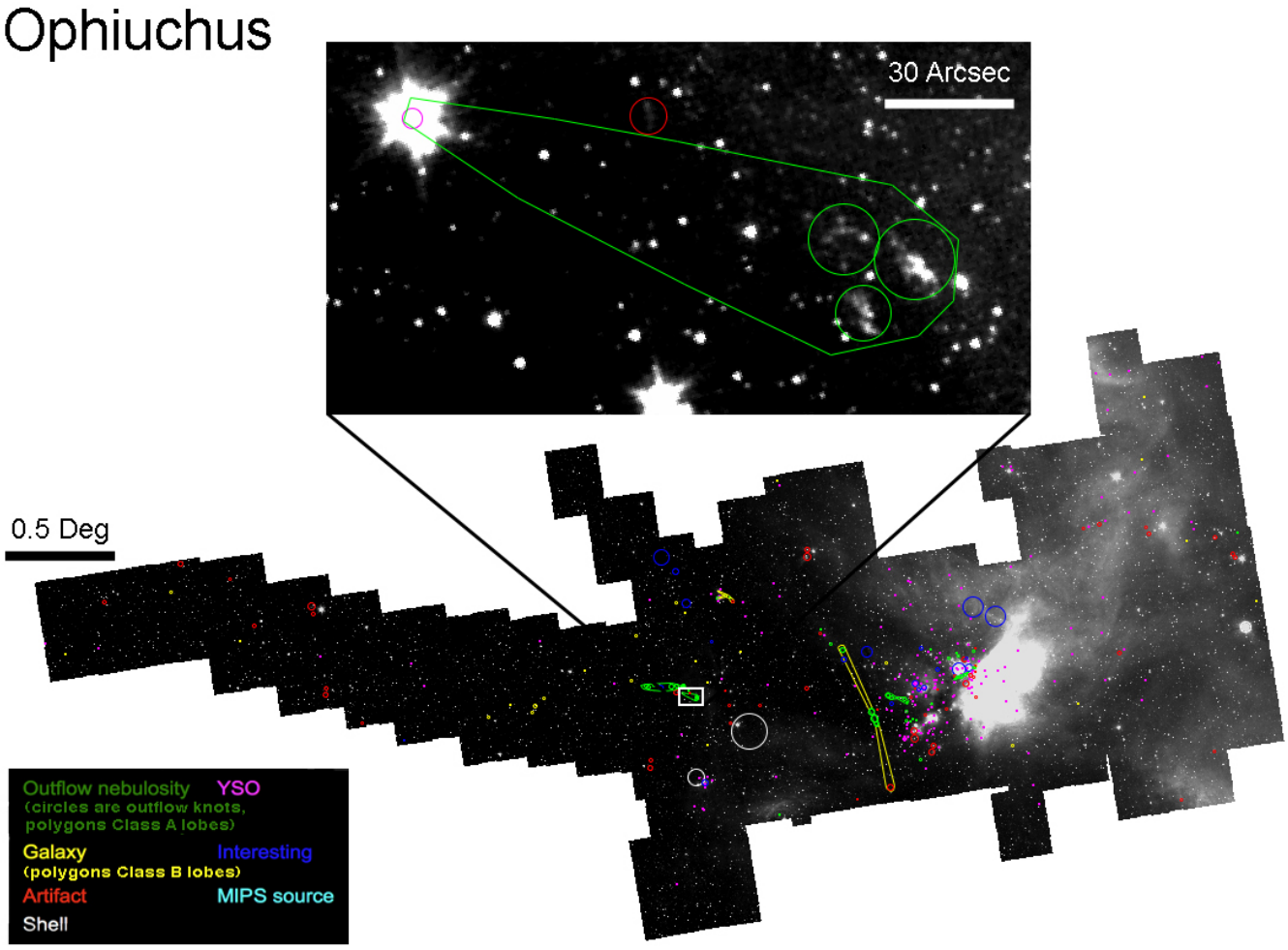

Fig. 12.— Complete mark-up from search for outflow nebulosity and lobe characterization showing the entire Ophiuchus molecular cloud. The enlarged image in the *upper* panel shows Oph-2a lobe. Unlike the other images in this series, this figure shows YSOs marked by us in the search exercise and also those from the c2d YSO catalog

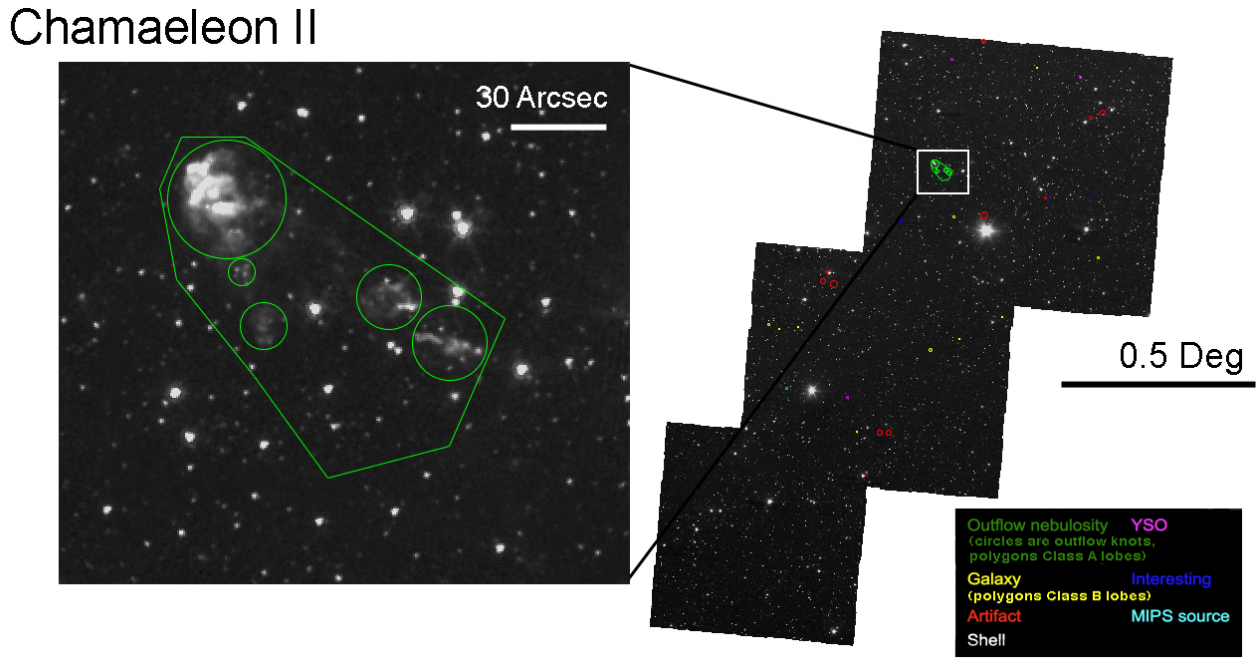

Fig. 13.— Complete mark-up from search for outflow nebulosity and lobe characterization showing the entire Chamaeleon molecular cloud. The enlarged image in the *upper left* panel shows Cha-1a lobe

4.2. Characterization of Outflows and Driving Sources

In this section I briefly discuss the abundance and distribution of outflows and their properties, I discuss the YSO content in each cloud, and we then attempt to understand how our sources are different from the total YSO population of the cloud.

4.2.1. Description of Outflow Properties

We find 86 lobes in the Spitzer data, with 72% in Perseus, 8% in Serpens, 19% in Ophiuchus, 1% in Chamaeleon II, and 0% in the Lupus molecular clouds. The clouds sit from 125 ± 25 to 260 ± 10 pc from us, and we see that roughly 80% of the outflows are at distances of > 200 pc. That is, there is a higher abundance of outflows at further distances from us in the Milky Way. We can also construct systems of lobes about a certain source, resulting in 45 different outflow systems of one or more lobe, where 58% are bipolar systems consisting of at least 2 lobes, one on each side of the central source, and 42% had only detections on one side of the suspected source. In terms of morphology, we see 3 cases of "S-shaped" outflows in Perseus, but these shapes occur at distances no greater than 0.15 pc from the source. We find lengths of outflows in our survey range from 0.03 pc up to ∼2 pc (see Table 10), where the longest outflow lobes in Perseus as well, and also outflow areas ranging from thousandths of pc^2 to $\sim 45 \times 10^{-3}\,pc^2$. In later steps we attempt to find a correlation between these properties and the YSO.

4.2.2. Characterization of YSO Content in Clouds

The absolute number of sources from the work by Evans et al. (2007) and their various classes (Sect. 1.2.1) are given in Table 8. We see that Perseus has overall the highest number of YSO candidates, an environment of 251 sources: 32% are Class I, 12% Flat SEDs, 51% Class II, and 5% Class III. NGC1333 alone has a total of 121 YSOs associated with it, the highest of the cluster regions, where 50% (60 of 121) are from the younger Class I and Flat groups. In contrast, we see that IC 348 has 73 YSO candidates, where Class I and Flat sources comprise only 20% (15 of 73) of all YSOs. This could be explained as IC348 having an older population of YSOs which have already gone through their outburst phase. Serpens has a total of 238 sources: ∼15% (36) Class I, 10% (23) Flat spectrum, 60% (142) Class II, and ∼15% (37) Class III. We see that the two subregions in Serpens are very similar in YSO content, where more than half of both regions are mostly Class II sources (42 of 82 for Cluster A, and 37 of 60 for Cluster B). It is also interesting that per pc^2, Serpens actually has a higher number of YSOs than any of the other c2d molecular clouds. Ophiuchus is the second most active region after Perseus with a total of 292 YSOs, with 12% (35) Class I, 16% (47) Flat spectrum, 60% (176) Class II, and 12% (34) Class III. Chamaeleon II and Lupus, as before, are somewhat less exciting when compared to the other clouds when looking at the paucity of young YSO sources in these complexes, where only 7 Class I, 11 Flat, 71 Class II, and 31 Class III YSO sources are given for both (a total of 120 sources).

4.2.3. Description of Outflow Sources

Figures 14a, b, and c are histograms that represent the distribution of spectral slopes, bolometric temperature, and bolometric luminosity for the sources we determined as outflow generators. There are three samples depicted in the figures: (1) the green distribution represents the entire 1024 YSO sample from the c2d *Spitzer* Legacy group, (2) the 33 sources that we suspect drive outflows in gray, and (3) the 22 highest in quality of these in dark gray. The high quality sources are those that are Class A and rated as having a definitely having a certain YSO as its source (see Sects. 3.4 and 3.5). For all plots in Figs. 14a–c , the bottom panel is provided as a zoomed in version of the top panel, in order to more clearly see the distribution in these properties for our suspected outflow sources. It is also important to note that in cases where the above parameters were not defined by the c2d catalog, they were not included in our outflow source sample sample.

We begin by analyzing the properties of the complete YSO group, and compare them to the YSOs driving outflows we detect in our survey. Figure 14a is a histogram of the spectral slope (α) for the three samples of YSOs. We see that the total YSO population has values ranging from +4 to −2, with the mode sitting at −1. This histogram indicates that the dataset is not symmetric, but is somewhat left-skewed. Our smaller outflow-driving sample (gray) is distributed over slopes ranging from −0.5 to +3.5, and our high quality source associations (dark gray) are also well distributed over this range. From this figure, we can conclude that the sources with outflows are redder in terms of α than the global YSO population.

Looking to Fig. 14b, we see that for the complete c2d YSO population, the bolometric temperatures peak at > 1000 K, with temperatures ranging from low tens of K to almost the tens of thousands K. Our small subset of outflow sources, on the other hand, only has bolometric temperatures from the tens of K, reaching up to 1000 K, with peaks at < 100 K. This tells us that outflow drivers are cooler as a whole than the larger YSO catalog. The last histogram depicts the distribution of bolometric luminosities, in units of solar luminosity, for the entire sample of YSOs and our specific sources associated with outflow activity. Whereas the two previous graphs showing the complete YSO sample were right-skewed, here the total sample is almost symmetric about $L_{\rm bol} \sim 10^{-1}$. Interestingly, the subsample of suspected outflow-driving sources seem to be more luminous than the median value of the entire YSO catalog, lying more on the right side of the horizontal axis. Also, the peak of both the outflow-driving sources plus the higher quality sources is around 1 $L_{\odot}$.

4.2.4. Interpretation of Distribution of YSO Properties

The first conclusion we gather from the histograms is that the sources we suspect to drive outflows are more reddened and cold, as compared to the global YSO population. Both the spectral slope and the bolometric temperature are indicators of stellar age, as discussed in Sect. 1.2.1. Either by looking at the slope of the SED, or calculating the bolometric temperature from the

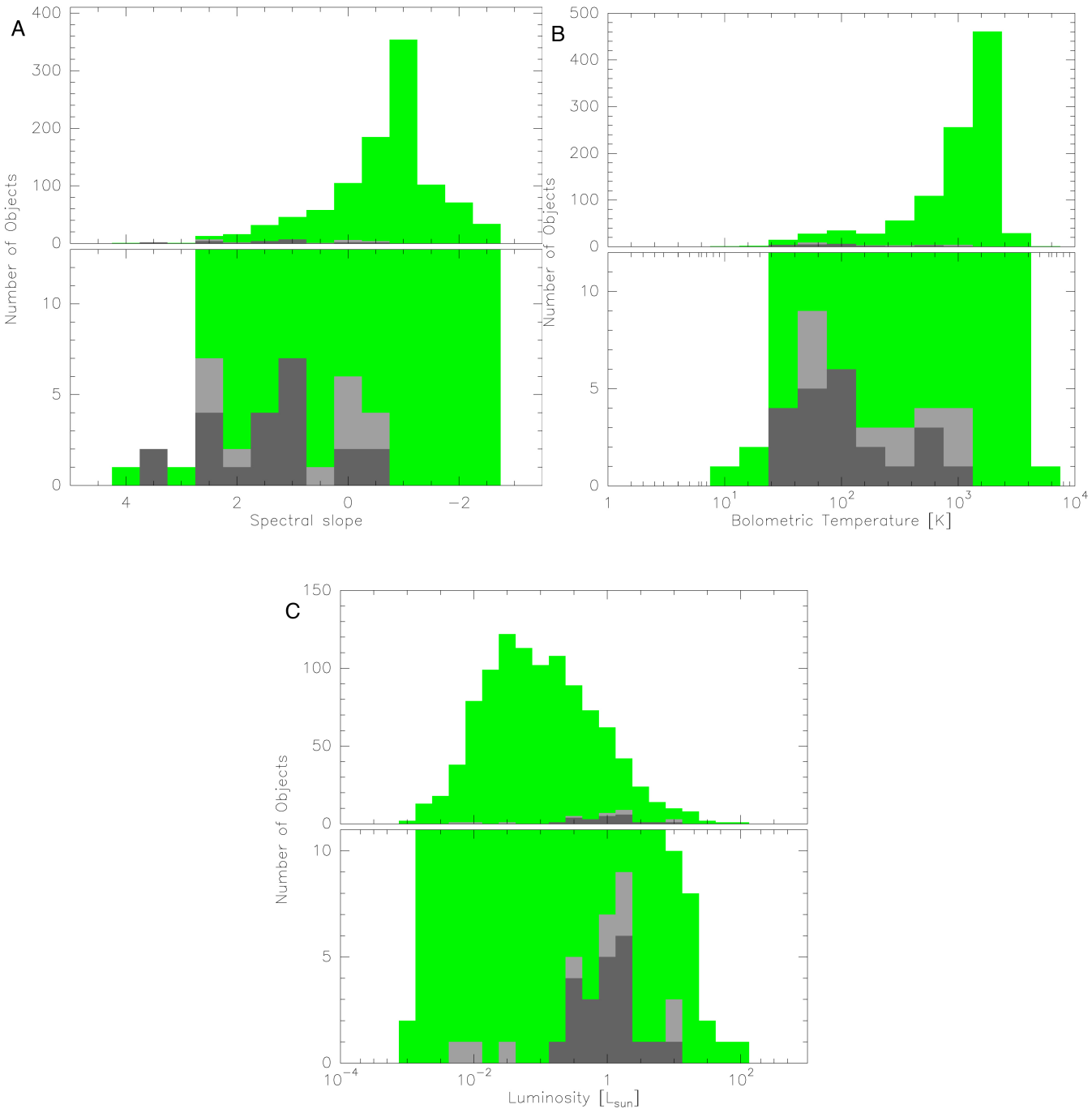

Fig. 14.— Distribution of objects with spectral slope (**A**), bolometric temperature $T_{\rm bol}$ (**B**), and bolometric luminosity $L_{\rm bol}$ (**C**). The *green* show the full YSO population, *light gray* show the full outflow-driving YSOs subpopulation, and the *dark gray* show the highest quality outflow-driving YSO sample. The *bottom* panels are zoomed in portions of the *top* panels to show our rather small sample (from 22 to 33) compared to the total YSO catalog from c2d (1024)

mean frequency of the observed spectrum, we can gauge how old the outflow sources may be. Considering the slope, we see that most of the outflow-driving sources are Class I sources, i.e., $\alpha > 0$. These are suspected to be the youngest in this scheme, where the positive slope indicates the presence of a circumstellar envelope. We also know that the colder YSOs are probably younger as well. Thus, both methods tell us that it is possible for our sources to be of the right age to power outflows.

Somewhat more difficult to interpret are the results from the luminosity histogram in Fig. 14c. We find that the sources with outflows are more luminous on average than the entire catalog of YSOs, where there is an under-abundance of low-luminosity outflow sources. This may be due to an observational bias, since less luminous sources will likely drive less obvious outflows, and thus be overlooked or simply not detected by our survey. If this low abundance of lower luminosity sources results not from a bias, but is indeed a real effect, then that would mean these low $L_{\rm bol}$ sources have a shorter outflow producing phase than the more luminous stars, and are thus harder to observe.

4.3. Comparison of Outflow Activity in Clouds

We now aim to characterize the difference in outflow activity, i.e., the absolute number of outflow knots we detect and their areas over the entire cloud, as well as on the scale of individual regions within these clouds. For the following descriptions, we use the regions in Table 4, which gives the boundaries we use to evaluate the five c2d clouds, along with their physical sizes. Our regions were drawn to include most of the IRAC knots we identified around the well known smaller dark clouds in each cloud (e.g., L1448 in Perseus, and L1688 in Oph), and note that these differ slightly from the regions described by the c2d group (Evans et al. 2008).

4.3.1. Trends in Activity in Clouds

Figure 15 shows numbers of knots, outflow areas and lobes with respect to the different classes of YSOs: the panels from left to right increase in age of the YSO, Class I, Flat, Class II, and Class III as described on Sect. 1.2.1. The different points, a color and symbol assigned to each cloud, represent the different regions within the cloud. The final column is then the sum of the previous four panels, over the total number of YSOs. Also plotted in the last column are dashed lines that represent a range of slopes (differing by a factor of 2). The points that fall along these lines have the same number of knots (area or number of lobes) per star in the sample.

As with any plotting scheme, we wanted to see if a correlation could be found. For example, it would be interesting if we found the same correlation between knots (area or number of lobes) and number of Class I objects for all the clouds. This would mean that this class of YSOs is the most responsible for the outflow activity we detect. Unfortunately all plots show a large amount of

scatter, where no striking trends stand out and we cannot point to a single class as the main factor of the observed outflows. It is surprising though that the best correlation we find is that showing number of outflow knots versus number of Class I YSOs in Perseus (top left), and not the plots of outflow area or number of lobes. We expect the knot area to be a better indicator of trends than simply the absolute number of knots we find. The outflow area is a more physical measure of activity in the clouds, where the number of knots on the other hand depends sensitively on how crowded the region is; we draw more small knots in a congested area of outflow knots, as opposed to a sparse region where we can more easily include objects into groups.

There however appears to be some correlation within each cloud. For example as stated above, the best correlation we find is between number of knots found versus number of Class I YSOs in Perseus. This correlation is also seen for Serpens, although it has a shallower slope, where we see that both subregions lie along the same line. When looking at the rightmost top plot, we see that certain points stay relatively close to each other and therefore can be separated into three groups based on their ratio of knots to all YSOs: (1) the cluster of red Perseus squares that have a high knot to YSO ratio (> 2 knots per star), (2) the small grouping of regions with an intermediate knot to YSO ratio, and (3) the collection of points that have a low knot to YSO ratio (< 0.5 knots per star). The cloud regions that occupy these groups are given in Table 9. It is worth noting that we did not find a single YSO class that is obviously responsible for the outflow activity, and therefore we consider the total number of YSOs.

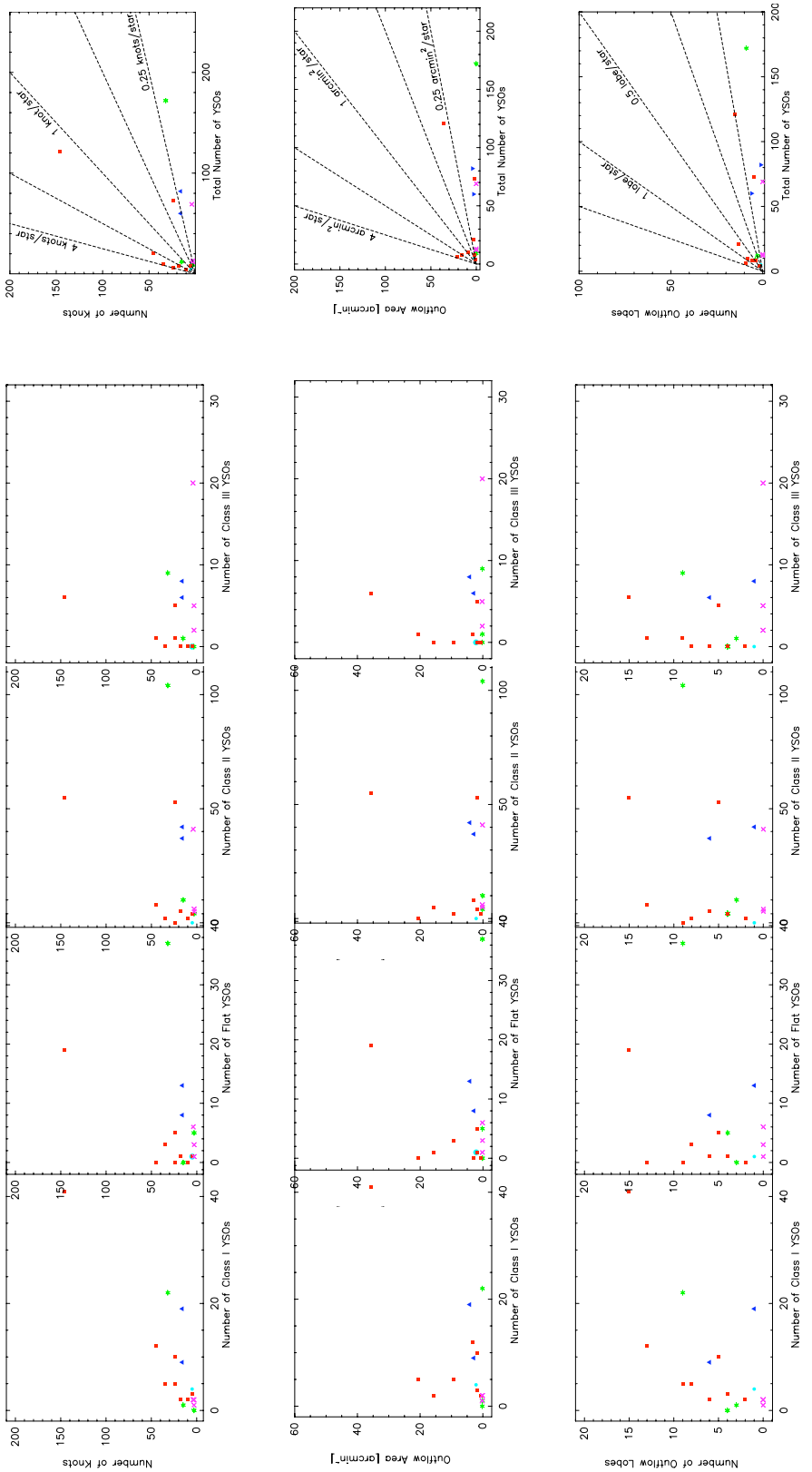

Fig. 15.— Relationships between number of knots (*top row*), outflow area (*middle row*), and number of outflow lobes (*bottom row*) and different classes of YSOs. The final column for all row shows the ratios of outflow parameters to the entire YSO population. The dashed lines in the last column represent a range of slopes (differing by a factor of 2), where points that fall along these lines have the same number of knots (area or number of lobes) per star in the sample. Legend: Perseus *red square*. Serpens *blue triangle*. Ophiuchus *green star*. Lupus *magenta cross*. Chamaeleon *cyan circle*

4.3.2. Interpretation of Activity in Clouds

In this section we further explore the trends found in the three groups by testing a few hypotheses, which may point to reasons for the changing knot-YSO correlation. Namely, we test if the age or stellar density play a role in the trends we see. As discussed in Sect. 1.2.1, we expect to find outflows from the younger stars in the YSO population, and thus a higher fraction of young objects may easily explain the more active areas in the clouds. By stellar density, we mean the spatial distribution (per parsec^2) of YSOs, which may affect the outflow activity we detect. The distribution of stellar classes in all clouds are shown in Fig. 17.

We first check the changes in age, as characterized by the number ratios between Class I and all YSOs (Fig. 16a). A region is supposedly young if this ratio is large, since Class I stars are thought to be the youngest stars. In this plot we find that the ratio [N (knots) / N (YSO)] is somewhat correlated to the age of the region. That is, if a region has more knots per YSO, it will also probably have a larger fraction of Class I sources. The relation grows stronger if we disregard Group 2, including the Chamaeleon region which has a high uncertainty. From this we see that younger regions are more likely to have a larger number of outflows and thus more knots.

Next we test if the material density gives any insight into the groups, by plotting the number ratio of knots to YSO versus the stellar population density, which is found by dividing the total number of YSOs in a given region by its linear size, as seen in Fig. 16b. From this we see that indeed the stellar density plays a role in the knots production. We can think of the stellar density as controlling the likelihood that an outflow from a given star can be seen, since the dense gaseous material associated with crowded star forming regions will inhibit the outflow from extending away from its source. Therefore, a low stellar density should give a larger outflow area, and thus produce more detectable knots. The length of outflow may also be influenced, if the surrounding material is also dilute, meaning that an outflow can travel further without being impeded much by the medium, and thus shock more material along its path. A clear example of this is the L1448 dark core in Perseus (see Figs. 6 and 17). Here we see that it is a young cluster, with a low star density, and has more knots per YSO, sitting at the far right in Fig. 16b. This points to the fact that generally regions with few YSOs have the ability to produce many outflows.

We must note here that the two tests we performed above may not be completely unrelated. That is, there may be some degeneracy between the age probed in the first test and the density probed by the second. We can understand this from the fact that as stars age they move from their birthplaces, so an older population will have spread away from each other thus making a less crowded stellar environment from which, by the above argument, outflows can be better observed. The conclusion from our tests show that we should expect to see more outflow activity in the form of knotty objects in cloud regions with a higher fraction of sparsely distributed young sources. In the next section we discuss how the properties of these sources are related to various properties of the outflow lobes we are able to trace.

Table 9. The three groups that emerge from Fig. 15, with ratio of number of knots to all YSO shown

	Group 1	Group 2	Group 3
N (knots)/N (YSO)	$N > 2$	$2 > N \geq 1$	$N < 1$
	L1448	IRAS12522	L1688
	L1455	L1689	L1709
	B1	NGC1333	IRAS03271
	B1 ridge		IC348
	B5		Cluster A
			Cluster B
			Lupus I, III, IV

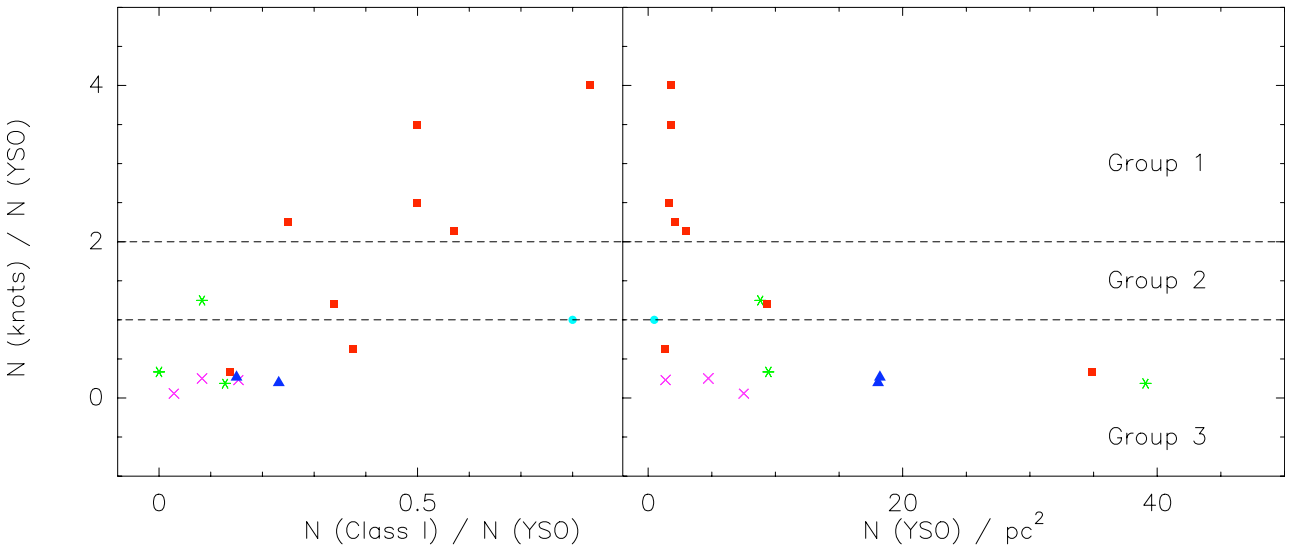

Fig. 16.— The groups from Fig. 15 and Table 9. (*left*) The plot of the number of knots per YSO and the ratio of Class I to all YSOs shows some correlation, where we find that a region with more knots per YSO will probably have a larger fraction of Class I sources. (*right*) Here, number of knots per YSO is plotted against the YSO density and we see that lower stellar densities are still able to produce many knots per YSO. Legend: Perseus *red square*. Serpens *blue triangle*. Ophiuchus *green star*. Lupus *magenta cross*. Chamaeleon *cyan circle*

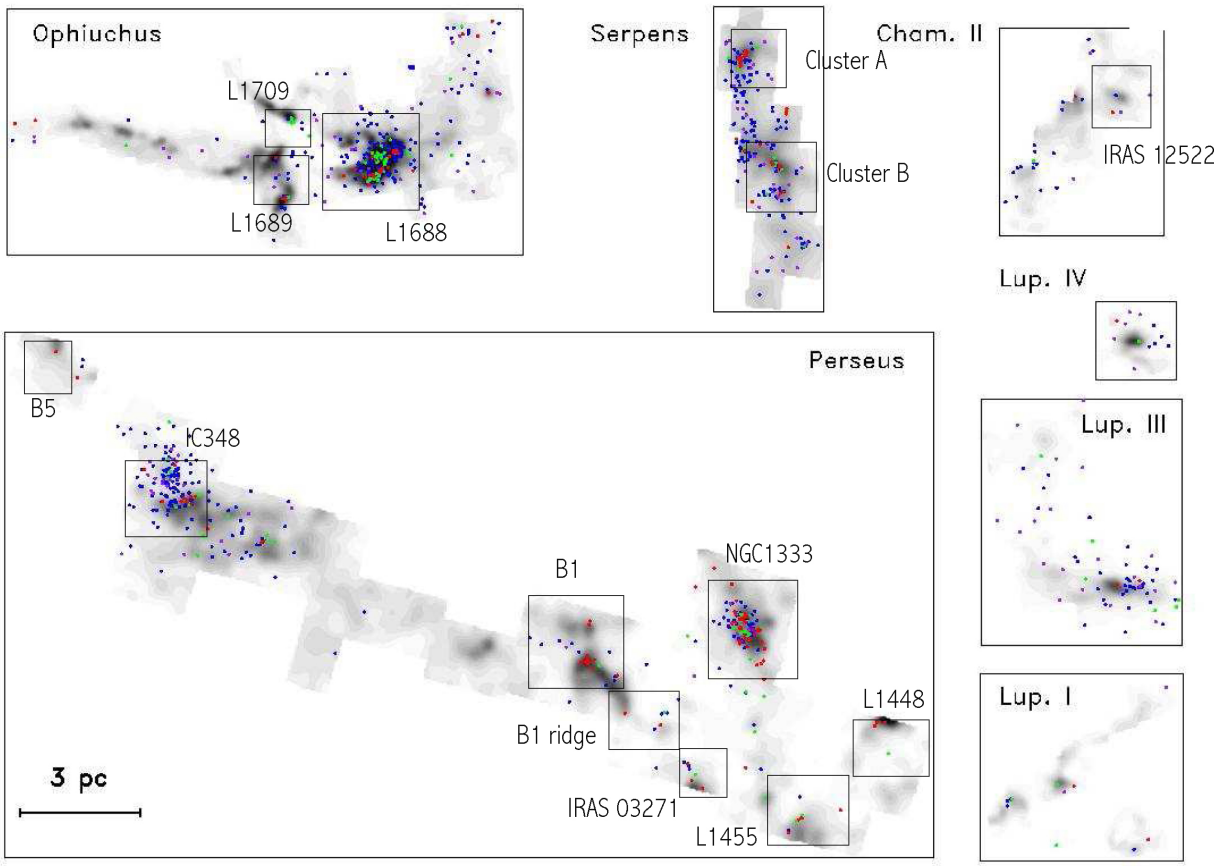

Fig. 17.— Extinction maps of all clouds in the survey, with the 3 pc scale bar showing the same absolute size scale for the clouds. The subregions we examined are also shown for each cloud. The complete "From Molecular Cores to Planet-Forming Disks" catalog of YSOs is also displayed, with the following colors representing Class of YSO: red (Class I), green (Flat SED), blue (Class II), and purple (Class III). From Evans et al. (2008)

4.4. Relationship Between YSO and Outflow Lobe Properties

This survey is the only one of its kind that simultaneously looks at sources and outflows from a single dataset (IRAC and MIPS data from *Spitzer*). As we show below, from our survey we are able to show that outflow area increases not only with YSO luminosity (can be thought of increasing with mass as well), but also that area decreases with age. These results confirm past hypotheses and allow us to use outflows to precisely assess the age (as well as size) of embedded YSOs during their development. Strikingly we find that these relationships are consistent in 5 unique molecular clouds, unlike other inconsistent and inhomogeneous studies.

Above we looked at the collective YSO population in relation to Spitzer outflow lobes. Here we discuss the relationship between the properties we measure for the outflow lobes and the properties of their suspected sources. We attempt to find trends between physical properties of the outflow activity (number of knots, area in knots, lobe length) and the observed properties of the YSO. Table 10 gives the properties of each lobe we found in the survey, with the quality of the lobe and source association, also including the characteristics of the suspected source. A note here that the lengths given are calculated from the suspected source to the furthest knot and does not take the shape of the polygon into account. The array of figures in Fig. 18 can be understood in the following way: every source has one or more lobes associated with it. The lobes may be of high or low quality depending on their score from our previously discussed rating regime. If the lobes are high quality, then they are represented by one red marker, low quality by one blue marker, where the source will have only one red and one blue marker for however many lobes may be assigned to it. The line that connects the two markers simply acts as visual representation of the uncertainty in outflow properties for that particular source. If only high quality or low quality lobes exist, then that marker is shown by itself with no line to connect to either the low or high counterparts, respectively. Overall, we found 33 outflow systems that had a source that was described in the c2d YSO catalog, consisting of one or many lobes. Twenty-two (67%) of these systems have at least one high quality lobe.

Let us first evaluate the luminosity plots in Fig. 18, by drawing a hypothetical line at 1 $L_{\odot}$ and one at 15×10^{-3} pc^2. Taking the case of luminosity versus outflow area (center) we see that 48% of high quality markers (red cross) lie within these boundaries, where no high quality markers below this luminosity threshold are found to have outflow areas greater than 15×10^{-3} pc^2. Only sources with $L > 1\,L_{\odot}$ are able to produce outflow areas above the area boundary, but do not necessarily do so. This trend occurs for the lower quality outflow systems as well, but with an outflow area threshold of around 40×10^{-3} pc^2. If we evaluate boundaries at 1 $L_{\odot}$ and 0.4 pc for the luminosity versus length panel (top right) we see that 48% of high quality sources lie below these limits. If we take the low quality lobes (blue triangle) into account, we can say that all $L < 1\,L_{\odot}$ sources are always confined to lobe lengths of < 1 pc. Conversely, only sources with $L > 1\,L_{\odot}$ are capable of generating outflows up to 2 pc in length, where the longest outflow at ~ 2 pc has a luminosity of $L \sim 10\,L_{\rm bol}$. This trend is echoed in the first plot of this series, for luminosity versus number of knots. It is not as obvious as the other two plots, but we do see that both high and low quality

objects with $L < 1\,L_{\odot}$ (bottom right corner) do not produce outflows with more than 10 outflow knots. These sorts of trends are at first glance what one would expect, since the lower luminosity objects are thought to still be surrounded by their natal envelopes, and thus cannot produce easily detectable outflows. In general, we can thus say that luminosity is a necessary but not sufficient condition for greater outflow lobe length and knot area, which is expected as $L \propto M$ and larger stars will produce more massive outflows, and more knots.

Next we discuss the temperature as plotted against outflow area. This panel has the most obvious correlation out of all the plots in Fig. 18. If we evaluate the markers with lines at 200 K and 15×10^{-3} pc^2 we see that 71% of high quality markers fall below these boundaries. Additionally, we find that only sources of $T_{\rm bol} < 200\,{\rm K}$ can have outflow areas greater than the threshold, where only 14% of high quality objects fall within these limits. For the higher temperature objects, we find that no $T_{\rm bol} > 200\,{\rm K}$ sources, high or low quality, have outflow areas larger than 15×10^{-3} pc^2. This is exactly what we expect to see, since stars with high $T_{\rm bol}$ are thought to be older and have presumably already gone through an outflow stage. Thus, we no longer see much outflow nebulosity since outflow associated phenomena are transient, where we know that HH objects only last for a few thousand years.

The bottom row of plots depicts how the outflow properties may depend on the spectral slope. The slope is shown from positive to negative along the y-axis, where we can say that older sources are found to have $\alpha < 2$ slopes and younger sources have $\alpha > 2$ and are reddened. A cursory look at the plots shows no clear correlations between outflow lobe properties and source properties. However, if we disregard the far outlying point at 1 $L_{\odot}$ and $\sim 70 \times 10^{-3}$ pc^2 in the center panel, then we see a similar trend to the one described in the temperature versus area plot. By drawing a line at $\alpha = 2$ and one at 20×10^{-3} pc^2, we find that 62% of high quality sources lie in the top left corner of the plot. We also find that only 10% of high quality sources have outflow areas greater than 20×10^{-3} pc^2 and have $\alpha > 2$. We interpret this to mean that younger sources of $\alpha > 2$ can produce more outflow area than older sources with $\alpha < 2$, but do not necessarily have to, while older stars always have small outflows.

Since the area of the outflow activity and the length of each outflow lobe are fundamental parameters, its relationship to the luminosity and temperature of the central source is essential in order to investigate the nature of outflows. Our investigation finds in general that more luminous objects can have both larger outflow areas and power outflows to greater lengths, that cooler stars can have a large outflow area, whereas stars with shallower spectral slopes have smaller outflow areas. It also follows that the bolometric temperature is a better diagnostic tool to describe outflow properties than the spectral slope, since we see a better correlation in the former. This may be due to the fact that the spectral slope, as calculated by the c2d *Spitzer* Legacy Program, is a more complicated parameter, which depends on more factors than the derived bolometric temperature.

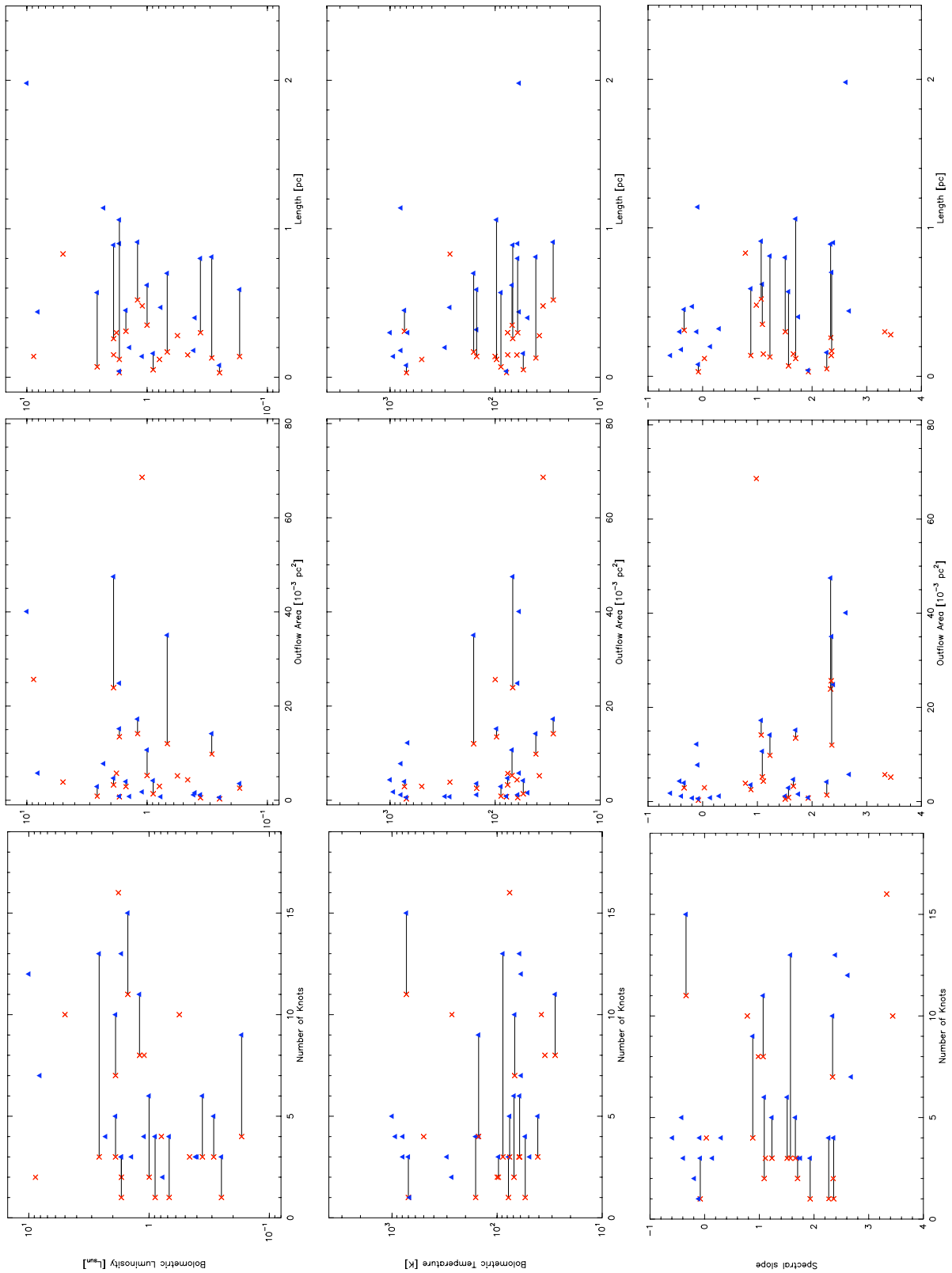

Fig. 18.— Relationship between stellar properties and outflow parameters. $L_{\rm bol}$, $T_{\rm bol}$, and α are plotted again number of knots, outflow area, and lobe length. *Red crosses* represent the high quality lobes associated to a source, and the *blue triangles* the low quality. The uncertainty between high and low quality is shown as a line between the low quality lobes in that outflow system and the higher quality lobes. Single markers are when there are either only high quality or low quality lobes in that system

Table 10. Outflow properties of all lobes surveyed in this work. When lengths are preceded by ≤, this indicates that these are lobes have no source, and thus the length is a lower limit

Name	Length [pc]	Knot area [arcmin^2]	No. Knots	Class	Source quality	Spitzer source [SST c2d+]	α	$T_{\rm bol}$ [K]	$L_{\rm bol}$ [$L_\odot$]
Cha-1a	≥0.31	2.17	5	A	4	N/A	N/A	N/A	N/A
Oph-1a	0.03	0.13	1	A	3	J162617.5–242315[b]	N/A	N/A	N/A
Oph-1b[a]		0.27	1	B	3	J162617.5–242315[b]	N/A	N/A	N/A
Oph-1c	0.14	1.34	4	A	3	J162624.0–242448	-0.59	930	1.1
Oph-1d	0.12	1.55	2	A	1	J162751.8–243145	0.03	500	0.79
Oph-1e	0.12	0.68	2	A	1	J162751.8–243145	0.03	500	0.79
Oph-1f[a]		1.16	1	B	3	J162821.6–243623	1.23	41	0.29
Oph-1g	0.06	2.30	1	A	1	J162821.6–243623	1.23	41	0.29
Oph-1h	0.13	5.12	2	A	1	J162821.6–243623	1.23	41	0.29
Oph-1i[a]		2.12	1	B	3	J162821.6–243623	1.23	41	0.29
Oph-2a	0.18	0.87	3	A	1	J163221.0–243036	-0.39	790	0.41
Oph-2b	0.04	0.45	3	A	1	J163221.6–242839	N/A	N/A	N/A
Oph-2c	0.39	4.36	5	A	1	J163221.6–242839	N/A	N/A	N/A
Oph-3a[a]		0.29	2	B	3	J163135.6–240129	0.14	300	1.4
Oph-3b	0.14	0.32	1	B	3	J163135.6–240129	0.14	300	1.4
Oph-3c	0.08	0.23	2	B	3	J163134.3–240325	-0.08	700	0.25
Oph-3d	0.03	0.22	1	A	1	J163134.3–240325	-0.08	700	0.25
Per-1a	0.26	1.28	5	A	1	J032522.3+304514	2.34	68	1.9
Per-1b	0.19	3.24	2	A	1	J032522.3+304514	2.34	68	1.9
Per-1c[a]		3.64	1	B	3	J032522.3+304514	2.34	68	1.9
Per-1d	0.16	0.82	2	B	2	J032522.3+304514	2.34	68	1.9
Per-1e	0.10	0.72	2	A	2	J032539.1+304358	2.36	≤160	≥0.68
Per-1f	0.17	2.27	1	A	1	J032539.1+304358	2.36	≤160	≥0.68
Per-1g[a]		3.64	1	B	3	J032539.1+304358	2.36	≤160	≥0.68
Per-1h	0.48	1.34	7	A	2	J032536.5+304522	2.62	59	10
Per-1i	1.98	6.24	5	A	2	J032536.5+304522	2.62	59	10
Per-2a	0.35	0.99	2	A	1	J032637.5+301528	1.09	69	1.0
Per-2b	0.19	0.45[c]	1	B	2	J032637.5+301528	1.09	69	1.0
Per-2c	0.62	0.58	3	B	3	J032637.5+301528	1.09	69	1.0
Per-2d	≥0.90	4.70	13	A	4	J032743.2+301229	2.39	61	1.7
Per-2e	0.20	0.76	4	A	2	J032739.1+301303	2.68	59	8.1
Per-2f	0.44	0.33	3	B	3	J032739.1+301303	2.68	59	8.1
Per-2g	0.47	0.14	2	B	3	J032738.2+301359	–0.19	270	0.77
Per-2h	1.14	1.47	4	A	2	J032747.7+301205	–0.09	790	2.3
Per-3a	≥ 1.08	10.50	7	A	4	N/A[b]	N/A	N/A	N/A
Per-3b	0.10	0.12	2	A	1	J032845.3+310542	1.11	62	0.46
Per-3c	0.15	0.70	1	A	1	J032845.3+310542	1.11	62	0.46
Per-3d	0.14	2.68	1	A	1	J032837.1+311331	2.35	100	8.8
Per-3e	0.13	2.17	1	A	1	J032837.1+311331	2.35	100	8.8
Per-3f	≥0.60	2.13	12	A	4	N/A[b]	N/A	N/A	N/A
Per-3g	≥1.06	2.14	22	B	4	N/A[b]	N/A	N/A	N/A
Per-3h	0.24	0.10	2	B	3	J032917.2+312746	1.75	49	0.40
Per-3i	0.40	0.20	1	B	3	J032917.2+312746	1.75	49	0.40
Per-3j	0.30	0.10	3	A	1	J032923.5+313330	1.51	61	0.36

Table 10—Continued

Name	Length [pc]	Knot area [arcmin^2]	No. Knots	Class	Source quality	Spitzer source [SST c2d+]	α	$T_{\rm bol}$ [K]	$L_{\rm bol}$ [$L_\odot$]
Per-3k	0.80	0.05	1	B	3	J032923.5+313330	1.51	61	0.36
Per-3l[a]		0.03	1	B	3	J032923.5+313330	1.51	61	0.36
Per-3m	0.43	0.04	1	B	3	J032923.5+313330	1.51	61	0.36
Per-3n	0.28	0.23	6	A	1	J032951.8+313906	3.44	38	0.56
Per-3o	0.24	0.75	4	A	1	J032951.8+313906	3.44	38	0.56
Per-4a	0.12	2.18	1	A	1	J033015.1+302349	1.70	97	1.7
Per-4b	0.06	0.37	1	A	1	J033015.1+302349	1.70	97	1.7
Per-4c[a]		0.32	1	B	3	J033015.1+302349	1.70	97	1.7
Per-4d	0.09	0.70	1	A	1	J033030.2+302709[b]	N/A	N/A	N/A
Per-5a	0.48	7.85	7	A	1	J033121.0+304530	0.98	35	1.1
Per-5b	0.26	5.12	1	A	1	J033121.0+304530	0.98	35	1.1
Per-5c	0.30	1.01	4	A	1	J033218.0+304948	1.07	28	1.2
Per-5d	0.52	1.66	4	A	1	J033218.0+304948	1.07	28	1.2
Per-5e[a]		0.52[c]	1	B	3	J033218.0+304948	1.07	28	1.2
Per-5f[a]		0.07[c]	2	B	3	J033218.0+304948	1.07	28	1.2
Per-6a	0.21	0.58	8	A	1	J033317.9+310932	3.33	76	1.8
Per-6b	0.30	0.50	8	A	1	J033317.9+310932	3.33	76	1.8
Per-6c	$\geq$0.28	0.11	3	C	5	N/A[b]	N/A	N/A	N/A
Per-6d	0.07	0.16	3	A	1	J033316.7+310755	1.57	88	2.6
Per-6e	0.32	0.14	4	B	3	J033316.7+310755	1.57	88	2.6
Per-6f	0.57	0.25	6	B	3	J033316.7+310755	1.57	88	2.6
Per-6g	0.14	0.48	4	A	1	J033320.3+310721	0.88	150	0.17
Per-6h	0.12	0.02	2	B	3	J033320.3+310721	0.88	150	0.17
Per-6i[a]		0.17	3	B	3	J033320.3+310721	0.88	150	0.17
Per-6j	0.03	0.14	1	A	1	J033327.3+310710	1.93	78	1.7
Per-6k	0.04	0.02	2	B	3	J033327.3+310710	1.93	78	1.7
Per-6l	0.32	0.22	4	B	3	J033257.8+310608	0.30	150	0.012
Per-6m	$\geq$1.00	0.26	4	C	5	N/A[b]	N/A	N/A	N/A
Per-7a	0.05	0.38	3	A	3	J034355.0+320103	-0.42	1000	0.0055
Per-7b	0.09	0.40	1	A	3	J034355.0+320103	-0.42	1000	0.0055
Per-7c[a]		0.04	1	B	3	J034355.0+320103	–0.42	1000	0.0055
Per-7d	0.31	0.55	11	A	1	J034359.6+320154	–0.34	730	1.5
Per-7e	0.45	0.20	4	B	3	J034359.6+320154	–0.34	730	1.5
Per-8a	0.81	0.26	3	A	1	J034741.6+325144	0.78	270	5.0
Per-8b	0.83	0.47	7	A	1	J034741.6+325144	0.78	270	5.0
Ser-1a	$\geq$ 0.30	2.13	1	A	4	J182947.0+011627	-0.11	680	0.042
Ser-2a	$\geq$0.26	1.11	3	A	4	N/A	N/A	N/A	N/A
Ser-2b	0.15	0.57	3	A	1	J182906.8+003034	1.66	76	1.9
Ser-2c	0.15	0.25	2	A	3	J182906.8+003034	1.66	76	1.9
Ser-2d	0.05	0.24	1	A	1	J182909.1+003132	2.27	54	0.89
Ser-2e[a]		0.30	1	B	2	J182909.1+003132	2.27	54	0.89
Ser-2f	0.16	0.19	2	B	1	J182909.1+003132	2.27	54	0.89

[a]Extension to parent lobe, which is why length is not given

[b]No known source, or not considered as YSO in c2d catalog

[c]Artifact used to calculate length and knot area

5. Conclusions and Future Work

In the following I summarize the results from this work. First, I review the outcome of the search we conducted to identify outflow nebulosity in *Spitzer* images, and how we characterized the subsequent outflow lobes. Next, I describe the results from Sect. 4. I discuss the characterization and variance of outflow activity in different clouds and regions, in particular how peculiar the region of Perseus is. I also describe the relationships we found between outflow lobe parameters and properties of the driving source. I conclude with topics for further study.

The first component of this research was to identify protostellar outflows in the molecular clouds by searching through *Spitzer* images, and the second was to then characterize the results from the search. We found a total of 409 knotty objects in the clouds, manifestations of outflows from protostars. From these knots we were able to construct 86 lobes of outflows, where we can find an associated source for 89% of these. Using our classification scheme and assigned source criteria we could then characterize the outflows, finding that 42% of these 86 lobes are of the highest quality. We construct systems of lobes about a certain source, resulting in 45 different outflow systems of one or more lobe, where 58% are bipolar systems consisting of at least 2 lobes, one on each side of the central source, and 42% have no counterpart on the opposite side of the source. Of these systems, 33 have a source that was described in the c2d YSO catalog, and it is these that we use to analyze if stellar properties affect outflow properties. We find lengths of outflows in our survey range from 0.03 pc up to ∼2 pc, with area of outflow activity from thousandths of pc^2 to $\sim 45 \times 10^{-3}\,\mathrm{pc}^2$. The catalog we produce is one of the most comprehensive catalogs of IR-detected outflows and thus will enable a large amount of continuing subsequent work.

In Table 8 we see the outflow activity and stellar activity of each region in each cloud, as discussed in Sect. 4.1. We notice that in most cases, the Perseus molecular cloud is different from the other clouds. It has the most outflow activity, with 310 knotty objects detected and 62 outflow lobes could be detected. Perseus also has the most YSOs (251), as found by c2d, with the largest in physical area of all the clouds at 73.6 pc^2 and also the second highest YSO density. Of the outflow lobes, 42% received the highest confidence rating. Perseus was also interesting when we compared regions within the cloud. For instance, we see a clear difference in number of embedded Class I sources and "flat spectrum" YSOs in NGC1333 and IC348. We also see that IC348 has substantially less outflow activity than NGC1333. This suggests that IC348 is older than NGC1333, and thus we see a difference in outflow activity as well.

Next we compared the sources that drive outflows to the entire YSO sample in Sect. 4.2. Here we concluded that sources with outflows are more likely to have a spectral slope of $\alpha \geq 1$ than the full source sample, which peaks at $\alpha \sim 1$. In terms of bolometric temperature, we find that the outflow sources are more likely to have $T_{\mathrm{bol}} < 10^2\,\mathrm{K}$, as opposed the complete YSO catalog, which has a peak at $T_{\mathrm{bol}} > 10^3\,\mathrm{K}$. From this analysis we learned that sources that generate outflows have more positive α, which are normally associated with more reddened sources, and are cold as compared to the rest of the YSO population. Both these bolometric temperature and spectral slope are indicators of stellar age, and it is true that red, cold sources have been observed to drive

outflows. Thus the sources we suspect may be a certain age and at a specific point in this star formation phase.

We looked for relationships between outflow activity in all clouds and classes of YSOs in Sect. 4.3.1, but found no obvious trends. When looking closer, we found interesting correlations when looking at a single cloud, as opposed to the entire cloud sample. In Perseus for example, we saw a correlation between outflow knots and Class I YSO. To test this, we explored how this relation depends on age, as determined by ratios of YSO classes, and YSO densities. From this we found that younger regions are more likely to have a larger number of outflows and thus more knots. We also discovered that generally regions with few YSOs have the ability to produce many outflows. In summary, we found that we should expect to see more knotty outflow objects in cloud regions with a higher fraction of sparsely distributed young sources.

Finally, in Sect. 4.4 we examined each lobe in terms of number of knots, outflow area, and length. We then compared these properties to the properties of the driving YSO. Our investigation finds that objects with $L_{\rm bol} > 1 L_{\odot}$ can have both larger outflow areas up to 40×10^{-3} pc^2 and power outflows to greater lengths, up to 2 pc, but this is not a necessary outcome. Also, stars with $T_{\rm bol} > 200$ K have a maximum outflow area of about 20×10^{-3} pc^2 meaning that they produce smaller outflow areas than sources with cooler temperatures. Another finding is that stars with spectral slopes of $\alpha < 2$, thought to be older sources produce small outflow areas, with an upper limit of 20×10^{-3} pc^2.

Due to the amount and complexity of the data, this work is far from complete. I would like to look more into the outflow systems as a whole, and examine what factors dictate the occurrence of a bipolar outflow. In other words, what does it mean when lobes do not have a symmetric lobe emanating from the other side of the central source? In general, what does symmetry or the shapes of an outflow tell us about the outflow mechanism and/or the surrounding material? Also, we see that Perseus stands out among the other clouds in outflow activity. It would be interesting to investigate why this cloud is different from the others, and if the stars forming in Perseus act differently from stars forming in Serpens.

There are many other topics I would like to explore, among those are the questions about outflow morphology, or why there is such a variety in outflow shapes? There is also optical evidence for episodic ejections of gas from the YSO and this may affect the shapes we see. It may also be the case that the central source is not stationary, but moves relative to its surroundings. I would also like to compare our findings with other outflow surveys, even though they may be of inhomogeneous nature. In general, a multi-wavelength study of associated outflow phenomena is needed to better probe different parts of the outflow. For example, the work by Borkin et al. (submitted 2008) searched the Perseus cloud in CO, and the studies by Walawender et al. (2005), which catalogued HH objects in Perseus as well. It will be beneficial to compare what information these different wavelength regimes reveal about outflows to provide a more complete picture of this important phase in stellar development.

6. Appendix

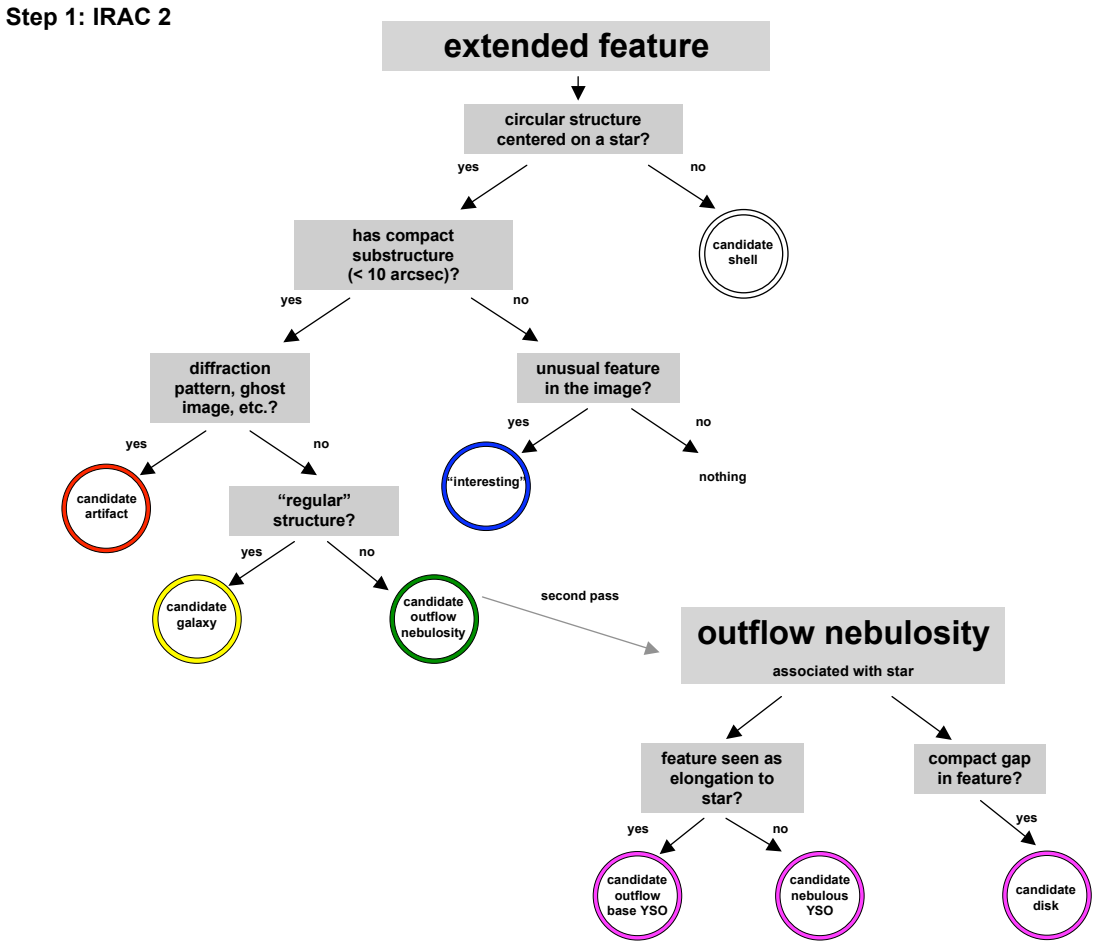

Fig. 19.— Flow chart depicting the first step in the search method

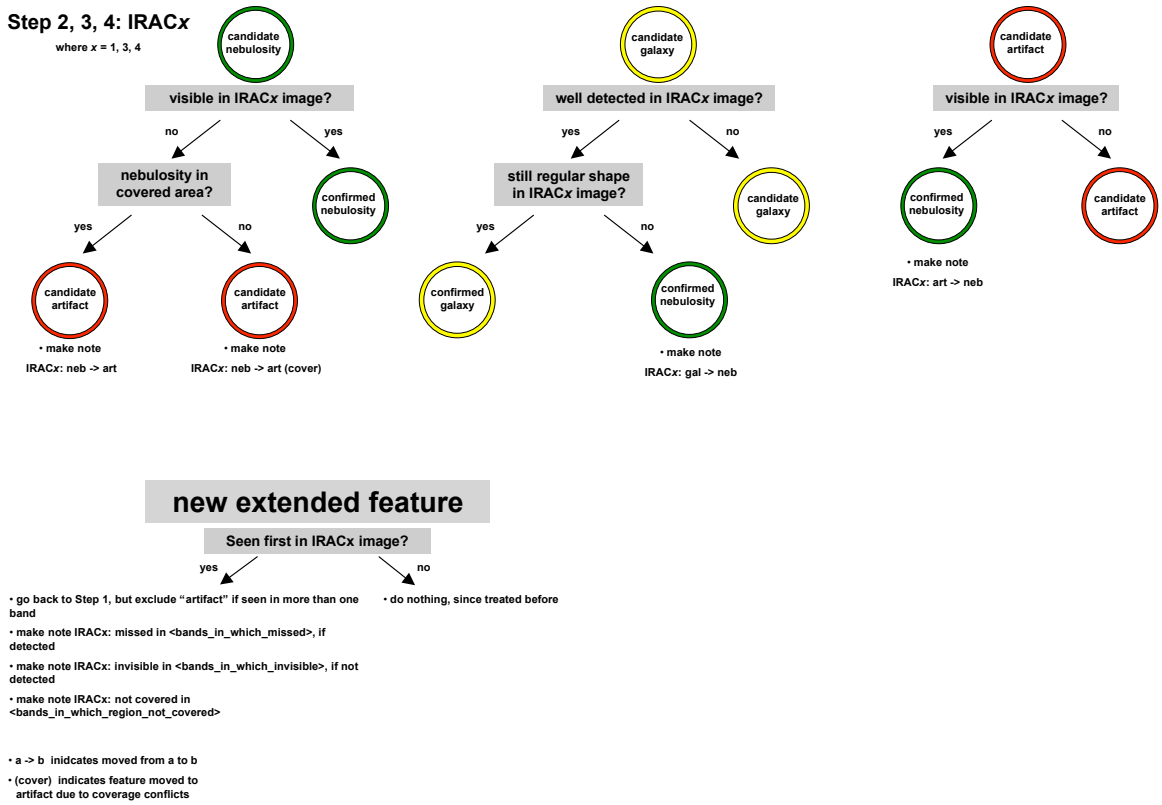

Fig. 20.— Flow chart depicting the remaining steps in the search method

Table 11. Tracing criteria and scoring for all Spitzer lobes identified in this survey

Region	Lobe name	Well sampled?	Non-confused region?	Bow shock shape?	Class	Source association
IRAS12522	Cha-1a	Y	Y	Y	A	4
L1688	Oph-1a	Y	Y	N	A	3
	Oph-1b[a]	Y	Y	N	B	3
	Oph-1c	Y	Y	N	A	3
	Oph-1d	Y	Y	N	A	1
	Oph-1e	Y	Y	Y	A	1
	Oph-1f[a]	N	Y	Y	A	3
	Oph-1g	Y	Y	N	A	1
	Oph-1h	Y	Y	Y	A	1
	Oph-1i[a]	N	Y	N	B	3
L1689	Oph-2a	Y	Y	N	A	1
	Oph-2b	Y	Y	N	A	1
	Oph-2c	Y	Y	Y	A	1
L1709	Oph-3a[a]	Y	Y	N	B	3
	Oph-3b	N	N	N	B	3
	Oph-3c	N	N	N	B	3
	Oph-3d	Y	Y	N	A	1
L1448	Per-1a	Y	Y	N	A	1
	Per-1b	Y	Y	N	A	1
	Per-1c[a]	N	N	Y	B	3
	Per-1d	Y	N	N	B	2
	Per-1e	Y	Y	N	A	2
	Per-1f	Y	Y	N	A	1
	Per-1g[a]	N	N	Y	B	3
	Per-1h	Y	Y	N	A	2
	Per-1i	N	Y	Y	A	2
L1455	Per-2a	Y	Y	N	A	1
	Per-2b	N	Y	N	B	2
	Per-2c	Y	N	N	B	3
	Per-2d	Y	Y	N	A	4
	Per-2e	Y	Y	N	A	2
	Per-2f	Y	N	N	B	3
	Per-2g	N	N	N	B	3
	Per-2h	Y	Y	N	A	2
NGC1333	Per-3a	Y	Y	Y	A	4
	Per-3b	Y	Y	N	A	1
	Per-3c	Y	Y	N	A	1
	Per-3d	Y	Y	N	A	1
	Per-3e	Y	Y	N	A	1
	Per-3f	Y	Y	N	A	4
	Per-3g	Y	N	N	B	4
	Per-3h	N	Y	N	B	3
	Per-3i	N	N	N	B	3
	Per-3j	Y	Y	N	A	1
	Per-3k	N	Y	N	B	3

Table 11—Continued

Region	Lobe name	Well sampled?	Non-confused region?	Bow shock shape?	Class	Source association
	Per-3l	N	Y	N	B	3
	Per-3m	N	Y	N	B	3
	Per-3n	Y	Y	N	A	1
	Per-3o	Y	Y	N	A	1
IRAS032	Per-4a	Y	Y	N	A	1
	Per-4b	Y	Y	N	A	1
	Per-4c	N	Y	N	B	3
	Per-4d	Y	Y	N	A	1
B1 ridge	Per-5a	Y	Y	N	A	1
	Per-5b	Y	Y	N	A	1
	Per-5c	Y	Y	N	A	1
	Per-5d	Y	Y	N	A	1
	Per-5e	N	Y	N	B	3
	Per-5f	N	Y	N	B	3
B1	Per-6a	Y	Y	N	A	1
	Per-6b	Y	Y	N	A	1
	Per-6c	N	Y	N	C	5
	Per-6d	Y	Y	N	A	1
	Per-6e	Y	N	N	B	3
	Per-6f	N	N	N	B	3
	Per-6g	Y	Y	N	A	1
	Per-6h	N	N	N	B	3
	Per-6i	N	N	N	B	3
	Per-6j	Y	Y	N	A	1
	Per-6k	N	N	N	B	3
	Per-6l	Y	N	N	B	3
	Per-6m	N	Y	N	C	5
IC348	Per-7a	Y	Y	N	A	3
	Per-7b	Y	Y	N	A	3
	Per-7c	N	Y	N	B	3
	Per-7d	Y	Y	N	A	1
	Per-7e	N	Y	N	B	3
B5	Per-8a	Y	Y	N	A	1
	Per-8b	Y	Y	N	A	1
Cluster A	Ser-1a	Y	Y	N	A	4
Cluster B	Ser-2a	Y	Y	N	A	4
	Ser-2b	Y	Y	N	A	1
	Ser-2c	Y	Y	N	A	3
	Ser-2d	Y	Y	N	A	1
	Ser-2e[a]	Y	Y	N	B	2
	Ser-2f	N	Y	N	B	1

[a]Extension to parent lobe

REFERENCES

Alcalá, J. M., Spezzi, L., Chapman, N., et al. 2008, Astrophys. J., 676, 427

Andre, P., Ward-Thompson, D., & Barsony, M. 1993, Astrophys. J., 406, 122

Bacciotti, F., Ray, T. P., Mundt, R., Eislöffel, J., & Solf, J. 2002, Astrophys. J., 576, 222

Bally, J. 2007, Ap&SS, 311, 15

Bally, J. & Lada, C. J. 1983, Astrophys. J., 265, 824

Bally, J., Reipurth, B., & Davis, C. J. 2007, in Protostars and Planets V, ed. B. Reipurth, D. Jewitt, & K. Keil, 215–230

Caselli, P., Benson, P. J., Myers, P. C., & Tafalla, M. 2002, Astrophys. J., 572, 238

Chen, H., Myers, P. C., Ladd, E. F., & Wood, D. O. S. 1995, Astrophys. J., 445, 377

Chrysostomou, A., Bacciotti, F., Nisini, B., et al. 2008, Astron. &. Astrophys., 482, 575

Dame, T. M., Ungerechts, H., Cohen, R. S., et al. 1987, Astrophys. J., 322, 706

Davis, C. J., Scholz, P., Lucas, P., Smith, M. D., & Adamson, A. 2008, Monthly Not. Roy. Astron. Soc., 387, 954

Eisloeffel, J. & Mundt, R. 1994, Astron. &. Astrophys., 284, 530

Evans, II, N. J., Dunham, M. M., Jørgensen, J. K., et al. 2008, ArXiv e-prints

Evans, II, N. J., Harvey, P. M., Dunham, M. M., et al. 2007, Spitzer Science Center

Greene, T. P., Wilking, B. A., Andre, P., Young, E. T., & Lada, C. J. 1994, Astrophys. J., 434, 614

Haro, G. 1952, Astrophys. J., 115, 572

Hartmann, L. & MacGregor, K. B. 1982, Astrophys. J., 259, 180

Harvey, P., Merín, B., Huard, T. L., et al. 2007, Astrophys. J., 663, 1149

Herbig, G. H. 1951, Astrophys. J., 113, 697

Herbig, G. H. & Jones, B. F. 1981, Astron. J., 86, 1232

Jørgensen, J. K., Harvey, P. M., Evans, II, N. J., et al. 2006, Astrophys. J., 645, 1246

Lada, C. J. 1987, in IAU Symposium, Vol. 115, Star Forming Regions, ed. M. Peimbert & J. Jugaku, 1–17

Lada, C. J. & Wilking, B. A. 1984, Astrophys. J., 287, 610

Ladd, E. F., Adams, F. C., Casey, S., et al. 1991, Astrophys. J., 366, 203

Lee, C. W., Myers, P. C., & Plume, R. 2004, Astrophys. J. Suppl., 153, 523

Lee, C. W., Myers, P. C., & Tafalla, M. 1999, Astrophys. J., 526, 788

Lee, C. W., Myers, P. C., & Tafalla, M. 2001, Astrophys. J. Suppl., 136, 703

Merín, B., Jørgensen, J., Spezzi, L., et al. 2008, Astrophys. J. Suppl., 177, 551

Myers, P. C. & Ladd, E. F. 1993, Astrophys. J. Letters, 413, L47

Padgett, D. L., Rebull, L. M., Stapelfeldt, K. R., et al. 2008, Astrophys. J., 672, 1013

Reipurth, B. 2000, VizieR Online Data Catalog, 5104, 0

Schwartz, R. D. 1975, Astrophys. J., 195, 631

Shu, F. H., Adams, F. C., & Lizano, S. 1987, Annu. Rev. Astron. Astrophys., 25, 23

Snell, R. L., Loren, R. B., & Plambeck, R. L. 1980, Astrophys. J. Letters, 239, L17

Stahler, S. W. & Palla, F. 2005, The Formation of Stars (The Formation of Stars, by Steven W. Stahler, Francesco Palla, pp. 865. ISBN 3-527-40559-3. Wiley-VCH , January 2005.)

Terebey, S., Shu, F. H., & Cassen, P. 1984, Astrophys. J., 286, 529

Velusamy, T. & Langer, W. D. 1998, Nature, 392, 685

Walawender, J., Bally, J., & Reipurth, B. 2005, Astron. J., 129, 2308

Wilson, R. W., Jefferts, K. B., & Penzias, A. A. 1970, Astrophys. J. Letters, 161, L43+

Zeilik, M. & Gregory, S. 1998, Introductory Astronomy and Astrophysics (Introductory Astronomy and Astrophysics, 4/e, published by Harcourt College Publishers, 1998; ISBN number: 0-03-006228-4)

Acknowledgements

I would like to thank Professor Tilman Butz for facilitating my project, Dr. Konrad Schiele for helping me transition to doing a master's thesis in the US, and Professor Alyssa Goodman at the Harvard-Smithsonian Center for Astrophysics for advising me on a specific project for this thesis. I would also like to thank Dr. Jens Kauffmann for advising me on a daily (and sometimes hourly) basis. Working with him was one of the most educational experiences and I'm grateful for his patience and his help. He also greatly helped in editing this thesis, where none of the results presented here would have been possible without his guidance and support. I kindly thank everyone at the Harvard-Smithsonian Center for Astrophysics in Cambridge for insightful discussions, and also Sarah Block for helping me with technical problems. Warmest thanks go to my parents and family, for helping me on my past science fair projects and always encouraging me during this one. Finally, I want to thank my partner Allen, the best physicist I know, for making this year bearable, and for his endless support during every step of this process.